

# A Review on Fabrication Methods, Characterization and Applications of Magnetic Iron Oxide Nanomaterials

T. K. Mandal\* and D. B. Roy

\* dr.mandal@iudehradun.edu.in

Received: July 2019

Revised: October 2019

Accepted: January 2020

ICFAI Tech School, ICFAI University, Rajawala Road, Central Hope Town, Selaqui, Dehradun, India.

DOI: 10.22068/ijmse.17.1.124

**Abstract:** Magnetic iron oxide nanomaterials (MIONs) have been extensively investigated for the various important applications. Coprecipitation, hydrothermal, high temperature decomposition of organic precursors, microemulsions, polyol methods, electrochemical methods, aerosol method, sonolysis and green synthesis processes for the fabrication of MIONs have been reviewed. Different characterization methods like XRD, SEM, EDX and TEM for the as prepared MION materials have been studied. Important applications of MIONs in the field of biomedical, nanorobotics and energy devices have also been addressed in this review. Target oriented drug delivery and hyperthermia applications of MIONs have also focused.

**Keywords:** Fabrication, Iron oxide nanomaterials, Nanorobotics, Drug delivery, Energy devices, Hyperthermia.

## 1. INTRODUCTION

Magnetic iron oxide nanomaterials (MIONs) have received much attention in recent years because of their applications in biomedical, nanorobotics and energy devices [1-5]. The biocompatibility of MIONs makes them suitable for biomedical applications, such as in cellular therapy, tissue repair, drug delivery, and magnetofection [1-3]. Recent investigations have focused on developing methods that synthesize magnetic NPs with vast potential including size, charge, stability, shape, and morphology [1-5]. In general, due to aggregation behavior, colloidal stability, cytotoxicity, surface coatings of the NPs are considered critical in nano research. Various biocompatibility tests have been done for polysaccharide-covered attractive NPs, for the human wellbeing as well as for the safety of the environment [4]. Using magnetic iron oxide nanomaterials (MIONs) in the treatment of cancer, as a chemotherapeutic anti-cancer drug, their efficacy as an anticancer agent was assessed [2]. Nanotechnology is at the leading edge of the rapidly developing new therapeutic and diagnostic concepts of all areas of medicine [3]. Recently, extensive research has been focused on nano-structured magnetite because it possesses unique magnetic and electric properties [5]. It

has also application in medical diagnosis and therapy, target drug delivery, magnetic resonance imaging, cancer hyperthermia treatment and as nano-sorbents in environmental engineering [4]. MIONs are commonly composed of magnetic elements, such as iron, nickel, cobalt and their oxides like magnetite ( $\text{Fe}_3\text{O}_4$ ), maghemite ( $\gamma\text{-Fe}_2\text{O}_3$ ) and cobalt ferrite ( $\text{Fe}_2\text{CoO}_4$ ). MIONs (<100 nm) thus can be manipulated under the influence of an external magnetic field.

The magnetic property of a material is based on its magnetic susceptibility ( $\chi$ ), which is defined by the ratio of the induced magnetization (M) to the applied magnetic field (H) [6]. In ferri- and ferromagnetic materials, magnetic moments align parallel to H, coupling interaction between the electrons of the materials result in ordered magnetic states. The  $\chi$  of these materials depends on their temperature, external field H and atomic structure. Ferri-or ferromagnetic materials, such as MIONs, become a single magnetic domain and therefore maintain one large magnetic moment [7]. The iron atom has four unpaired electrons in 3d orbital, thereby it has a strong magnetic moment.  $\text{Fe}^{3+}$  ions have five unpaired electrons in 3d orbital, and  $\text{Fe}^{2+}$  ions have four. When crystals are formed from iron atoms or  $\text{Fe}^{3+}$  and  $\text{Fe}^{2+}$  ions, they can be in ferromagnetic, antiferromagnetic or ferrimagnetic states. In the paramagnetic state

which is because of the presence of unpaired electrons in the material, all the magnetic moments are randomly oriented, so the crystal has no net magnetic moment. The crystal has a small net magnetic moment when an external magnetic field is applied, and the magnetic moment is zero when the field is removed [8]. In a ferromagnetic crystal, all the magnetic moments are aligned even without an external magnetic field [9]. In a ferrimagnetic crystal, two types of atoms with different magnetic moments are aligned in an antiparallel fashion, and the antiparallel moments have different magnitudes [10]. For an antiferromagnetic crystal, the antiparallel moments have the same magnitudes. Both magnetite ( $\text{Fe}_3\text{O}_4$ ) and maghemite ( $\gamma\text{-Fe}_2\text{O}_3$ ) are ferromagnetic. The magnetic energy of an NP is dependent on the direction of its magnetization vector. The direction that has the minimum magnetic energy is called anisotropy direction or easy axes, and it depends on the crystal structure of the particle. With the increase of the angle between the magnetization vector and the easy axis, the magnetic energy increases. The amplitude of this curve is called anisotropy energy [11].

Iron-based magnetic NPs such as  $\text{Fe}_3\text{O}_4$  have been received numerous attention due to their unique properties and potential applications in biomedical applications [12].  $\text{Fe}_3\text{O}_4$  NPs can potentially be used as magnetic targeted drug delivery carriers and magnetic resonance imaging (MRI) contrast agents due to their high saturation magnetization, low toxicity, and biocompatibility [13]. Magnetic properties of NPs can be tailored by their particle sizes and size distributions. NPs are ultrafine particles with their sizes ranging from 1-100 nm [7]. NPs have attracted considerable attraction due to their unusual and fascinating properties, with various applications, over their bulk counterparts [5,14]. Iron oxides are usually used as photocatalyst for the photocatalytic degradation of organic dyes due to their wide bandgap and high photosensitive nature. The crystal structure of  $\alpha\text{-Fe}_2\text{O}_3$  (hematite) is rhombohedral and it shows weak ferromagnetism at 300 K [15]. The hematite is an n-type semiconductor that has attracted substantial interest because of their potential applications in catalysis, pigments, gas sensors etc [9]. The other advantages of iron oxide

nanoparticles are nanorobotics, the 3D-printed nanorobots placed in liquids to eliminate toxins [4].

This review aims to address the different synthesis processes of MIONs, characterization of the as-prepared nanomaterials and its valuable applications in biomedical (targeted drug delivery, MRI contrast agent, antibacterial, hyperthermia and cancer treatment), nanorobotics (treatment of diabetes, treatment of cancer, cellular nanosurgery and gene-therapy) and energy devices (Li-ion battery, supercapacitor and chemical sensor). It also studies the correlation of the structure, property and applications of MIONs based on different synthesis routes. An environment-friendly green synthesis approach for the fabrication of iron oxide nanomaterials is also addressed herewith.

## 2. SYNTHETIC ROUTES

The preparation method has a very large effect on the size, shape, size distribution and surface chemistry of the magnetic nanoparticles and also on their applications [16]. Synthesis of the MIONs with optimized size and shape has always been a great challenge. Various synthesis methods have been explored to attain the MIONs with desired properties. Chemical synthesis has been the most common route. Some of the synthesis methods of iron oxide NPs are being addressed herewith.

### 2.1. Coprecipitation

Because of the easy implementation and use of less risky materials and simple procedures, the coprecipitation method is widely used in biomedical applications [8]. In this method, iron oxide particles are produced by an aging stoichiometric mixture of ferrous and ferric salts in aqueous media [14]. The size, shape, and composition of the particles depend on the salts used, the  $\text{Fe}^{3+}$  and  $\text{Fe}^{2+}$  ratio, the pH of the solution, the temperature, and the ionic strength of the media. The chemical reaction of  $\text{Fe}_3\text{O}_4$  formation can be written as:



According to the thermodynamics of this reaction, complete precipitation of  $\text{Fe}_3\text{O}_4$  should be expected between pH 9 and 14, while maintaining a molar ratio of  $\text{Fe}^{3+}:\text{Fe}^{2+}$  is 2:1 under a non-oxidizing oxygen-free environment. As  $\text{Fe}_3\text{O}_4$  is not very stable, in the presence of oxygen it can be oxidized into  $\gamma\text{-Fe}_2\text{O}_3$ . The reaction can be written as:



In order to prevent this oxidation in air, an oxygen-free environment is very important. To create such an environment, nitrogen is used by passing through the solution. The nitrogen through the solution not only can prevent the oxidation but also reduces the particle size. There are two steps in the coprecipitation process. Small nuclei are first formed in the medium when the concentration of the species reaches critical supersaturation, and it is followed by the growth of the crystal. In the later step, the solutes diffuse to the surface of the crystal, and the process is controlled by the mass transport. In order to produce NPs, the two stages are needed to be separated. For example, during the crystal growth step, the nucleation should not occur.

## 2.2. Hydrothermal Methods

Iron oxide NPs with controlled size and shape are technologically important due to the strong correlation between these parameters and magnetic properties [17]. Hydrothermal synthesis consists of various wet-chemical processes of crystallizing the substance in a sealed container from the high-temperature aqueous solution (generally in the range 130–250 °C) under high vapor pressure (generally in the range 0.3–4 MPa) [17]. This method has also been explored to develop dislocation-free single crystal particles, and grains formed in this method shown to have a better crystallinity than those from other methods. Therefore, the hydrothermal method is prone to obtain highly crystalline iron oxide NPs [17].

Different researchers have worked on the synthesis of iron oxide NPs using the hydrothermal method [18–25]. Ge et al. [19] investigated an

easy one-step hydrothermal methodology for the synthesis of  $\text{Fe}_3\text{O}_4$  NPs with controllable diameters, narrow size distribution and good magnetic properties. In this approach, the iron oxide NPs (15 to 31 nm) were synthesized by oxidation of  $\text{FeCl}_2 \cdot 4\text{H}_2\text{O}$  in basic aqueous solution under elevated temperature and pressure. The NPs showed high saturation magnetization in the range of 53.3–97.4 emu/g. The as-prepared iron oxide NPs utilized in many potential biological applications in cancer diagnosis and treatment [19]. Haw et al. prepared the  $\text{Fe}_3\text{O}_4$  NPs using a hydrothermal approach and the as-synthesized materials were explored in studying their application as MRI contrast agents [20]. A one-pot hydrothermal process has been reported to prepare  $\text{Fe}_3\text{O}_4@\text{Au}$  composite NPs for the applications in dual-mode magnetic resonance and computed tomography imaging. The  $\text{Fe}_3\text{O}_4@\text{Au}$  CNPs developed via the facile one-pot method reported to have promising potential for the dual-mode MR/CT imaging of different biological systems [21]. A facile, economical and environment-friendly hydrothermal method for fabricating  $\text{Fe}_3\text{O}_4$  and  $\alpha\text{-Fe}_2\text{O}_3$  NPs at 180 °C for 12 h respectively has been reported by Lou et al [22]. In their study, the diameters of  $\text{Fe}_3\text{O}_4$  and  $\alpha\text{-Fe}_2\text{O}_3$  nanocrystals were measured to be 5 and 20 nm, respectively. Also, the electrochemical performances of the  $\text{Fe}_3\text{O}_4$  and  $\alpha\text{-Fe}_2\text{O}_3$  nanoparticles as anode materials for Li-ion batteries were also determined. The first-discharge capacities of  $\text{Fe}_3\text{O}_4$  and  $\alpha\text{-Fe}_2\text{O}_3$  nanocrystals were reported to be 1,380 and 1,280 mAh g<sup>-1</sup> with the stability of about 96 and 75 mAh g<sup>-1</sup> after 20 cycles, respectively. These materials offered promise for developing alternative, high capacity negative electrodes for safer lithium batteries as energy storage and conversion materials [22]. Superparamagnetic  $\text{Fe}_3\text{O}_4$  NPs have been successfully synthesized under the hydrothermal conditions with the assistant of ionic liquid 1-hexadecyl-3-methylimidazolium chloride ( $[\text{C}_{16}\text{mim}]\text{Cl}$ ) by Liu et al [23]. It was found that  $[\text{C}_{16}\text{mim}]\text{Cl}$  acts as a stabilizer for the  $\text{Fe}_3\text{O}_4$  nanoparticles by adsorbing on the particles' surfaces to prevent the agglomeration. The obtained superparamagnetic  $\text{Fe}_3\text{O}_4$  nanoparticles by them have a saturation magnetization of 67.69 emu/g at 300 K [23]. Hydrophilic  $\text{Fe}_3\text{O}_4/\text{C}$

nanocomposites were prepared by a simple one-step hydrothermal reaction route using  $\text{FeCl}_3$  and glucose as raw materials, and sodium acetate as an alkali source. The phase structure, morphology, and composition were characterized. Prepared  $\text{Fe}_3\text{O}_4/\text{C}$  samples were demonstrated to show typical ferromagnetic behaviors and high removal capacities in removing the toxic  $\text{Cr(VI)}$  ions and organic pollutant Rhodamine B from wastewater, in addition to facile magnetic separability and good recyclability [24]. Iron oxide synthesized at  $190^\circ\text{C}$  through the hydrothermal method exhibited better magnetic properties due to the uniform distribution of spheres with particle size in the range, 18-25 nm [25].

### 2.3. High-Temperature Decomposition of Organic Precursors

The decomposition of iron precursors occurs in producing iron oxide nanoparticles in the presence of hot organic surfactants. The prepared particles through this method are with good size control and crystallinity, narrow size distribution and well dispersed as well [26]. For example, in the presence of octyl ether and oleic acid at  $100^\circ\text{C}$ , iron oleate can be produced through the decomposition of iron carbonyl [26]. Magnetite nanoparticles can be prepared with the decomposition of iron pentacarbonyl in the presence of oleic acid and aging at  $300^\circ\text{C}$ . The prepared particles show very good crystallinity with the particle size in the range of 4 to 16 nm [27]. The size and shape of the particles prepared through this method are evaluated through reaction temperature, time, precursors used etc. The surfactant on the surfaces of the particles is used to stabilize the colloid solution [28]. The thermal decomposition of iron carbonyl in the presence of octyl ether and oleic acid and using consecutive aeration can produce hydrophobic magnetite nanoparticles with narrow size distribution [29]. The decomposition of iron acetylacetonate with 1,2-hexadecanediol has been found in the presence of oleylamine and oleic acid at high temperatures [30]. The produced particles have sizes ranging from 4 to 20 nm. In organic solvent, the thermal decomposition of iron oleate and iron pentacarbonyl can produce particles with sizes ranging from 4 to 11 nm w.r.t different temperatures [30]. The

produced iron oxide nanoparticles are dispersible in some organic solvents. But most of these NPs are not dispersible in water. The decomposition of  $\text{Fe(acac)}_3$  or  $\text{FeCl}_3$  in refluxing 2-pyrrolidone can produce water-dispersible particles in acidic or basic media [31].

### 2.4. Sol-Gel Methods

This method involves the conversion of monomers into a colloidal solution (sol) that acts as the precursor for an integrated network (gel). The approach of sol-gel is cheap and it requires low temperature allowing the fabrication of fine-grained particles with homogeneous composition. As prepared materials through sol-gel have versatile applications in biomedicines, in energy devices and in electronics. Reda [32] used a sol-gel method to prepare  $\text{Fe}_2\text{O}_3$  nanoparticles in a silica matrix. As prepared materials were used as a photoanode to fabricate dye-sensitized solar cells (DSSCs). The author also studied the effects of annealing temperature as well as the concentration of  $\text{Fe}_2\text{O}_3$  on the efficiency of conversion of the  $\text{Fe}_2\text{O}_3$  based solar cell.  $\text{Fe}_2\text{O}_3$  nanoparticles are fabricated using a sol-gel method by Kayani et al. [33] also. The as-prepared NPs have been characterized by them through XRD, FTIR, SEM), TGA/DTA-DSC) and vibrating sample magnetometer. XRD study inferred the hematite phase of the prepared iron oxide NPs with an average crystallite size of the range from 34 to 36.7 nm [33]. Raja et al [34] have successfully synthesized the  $\alpha\text{-Fe}_2\text{O}_3$  nanoparticles via the sol-gel technique. They estimated the optical band gap energy as 2.55 eV. The values of coercivity and saturation magnetization are determined to be 3891 G and 0.4193 emu/g, respectively for the  $\alpha\text{-Fe}_2\text{O}_3$  nanoparticles. Sunder et al [35] explored the synthesis of g- $\text{Fe}_2\text{O}_3$  nanostructures by the application of the sol-gel method. Different morphological forms of g- $\text{Fe}_2\text{O}_3$  at different sizes and their improved magnetic and electrocatalytic behaviors can be used for potential biomedical applications.

### 2.5. Microemulsions

Microemulsions have been shown to be



an adequate, versatile, and simple method to prepare nanosized particles [36]. In water-in-oil microemulsion systems, the microdroplets of the aqueous phase surrounded by surfactant molecules are dispersed in a continuous oil phase [36]. The surfactant molecules limit the nucleation, growth, and agglomeration of the particles [37]. At the point when an iron salt solution is added to the microemulsion, the iron salt will be contained in the aqueous microdroplets. These microdroplets will continuously collide, coalesce, and break again. Therefore, if two reactants are added in the microemulsion, the precipitate of the resultant will be formed. The growth of the particles is progress of inter droplet exchange and nuclei aggregation. The precipitate can be extracted from the surfactants. Using aqueous core with aerosol-OT/n-hexane reverse micelles in microemulsion has produced the iron oxide nanoparticles with a very small size distribution [38]. The aqueous core is used to dissolve reactants. The solution of  $\text{Fe}^{3+}$  and  $\text{Fe}^{2+}$  salts with ratio 2:1 was dissolved in the aqueous core [39]. A deoxygenated solution of sodium hydroxide is used to achieve precipitation. The magnetite nanoparticles with smaller size and narrower size distribution have been produced in the presence of nitrogen gas at low temperatures. Because of the very small size (nm) of the aqueous core, the size of the formed particles is less than 15 nm. The distribution of the particles will be very narrow. The biggest advantage of the microemulsion method is that it can control the size of the particles by controlling the size of the aqueous core [40].

## 2.6. Polyol Methods

The iron oxide nanoparticles can be produced by the reduction of dissolved iron salts and direct precipitation in the presence of polyol. The polyols, such as polyethyleneglycol, have some good properties, such as the high dielectric constant, the ability to dissolve inorganic compounds, and the high boiling temperatures. They offer a wide range of operating temperature for the production of inorganic compounds. They are used not only as of the agents of reduction but also as the stabilizers, and they can control the growth of particles and prevent aggregation.

In the polyol method, a precursor is suspended in a liquid polyol. The suspension is stirred and heated to a given temperature that reaches the boiling point of polyol [41]. The precursor becomes soluble in the diol during the process, and then it is reduced to form metal nuclei that will form metal particles. The particles with the desired size and shape can be produced by controlling the kinetics of the process [42]. The yield of iron oxide nanoparticles produced by this method depends on the type of polyols, ferrous salts, concentration, and temperature. The size and yield of the particles are related to the reduction potential of the polyols. In a report, the non-aggregated magnetite nanoparticles have been produced by a modified polyol method [43]. Four different polyols, including ethylene glycol, diethylene glycol, triethylene glycol, and tetraethylene glycol, are used to react with  $\text{Fe}(\text{acac})_3$  at an elevated temperature. The non-aggregated magnetite nanoparticles with narrow size distribution and uniformed shape are only produced when using triethylene glycol [44].

## 2.7. Electrochemical Methods

The  $\gamma\text{-Fe}_2\text{O}_3$  nanoparticles with size ranging from 3 to 8 nm have been prepared by electrochemical method [45]. In this process, the particles are produced from an iron electrode in an aqueous solution of dimethylformamide and cationic surfactant [45]. The size of the particles is controlled by the current density. Electrochemical deposition can be used to produce  $\text{Fe}_2\text{O}_3$  and  $\text{Fe}_3\text{O}_4$  particles under oxidizing conditions [46].

## 2.8. Aerosol/Vapor Method

Aerosol methods, including spray and laser pyrolysis, are continuous chemical processes, and they are allowing for high rate production. A process in which a solution of ferric salts and a reducing agent in organic solvents are sprayed into a series of reactors, where the solvent evaporates and the solute condenses is called spray pyrolysis. The size of the original droplets controls the size of the produced particles [47]. Using different iron precursors in the alcoholic solution can produce maghemite particles with size ranging from 5 to 60

nm and with different shapes. Laser pyrolysis is a valuable method to reduce reaction volume. In the method, the non-aggregated particles with small size and narrow size distribution can be produced by using a laser to heat a flowing gaseous mixture of the iron precursor. The produced maghemite particles can have a size ranging from 2 to 7 nm and very narrow size distribution by controlling the experimental conditions. For example, maghemite nanoparticles with a size of 5 nm have been produced by continuous laser pyrolysis of  $\text{Fe}(\text{CO})_5$  vapors [48].

## 2.9. Sonolysis

The decomposition of organometallic precursors by sonolysis can also produce iron oxide NPs. Polymers, organic capping agents, or structural hosts can help to limit the particle growth. The rapid collapse of sonically generated cavities generates a very high-temperature hot spot, which allows the conversion of ferrous salts into magnetic nanoparticles. For example, a hydrosol of amorphous magnetite nanoparticles can be produced by the sonolysis of  $\text{Fe}(\text{CO})_5$  aqueous solution in the presence of sodium dodecyl sulfate [49]. Well-defined super magnetic iron oxide nanoparticles have been produced by sonolysis [50]. In the report, the produced particles are coated with oleic acid, a surfactant, and they can be dispersed in chitosan solution. The coated particles have a size of 65 nm, and they are very stable [51]. For applications, the particle size, size distribution, particle shape, and magnetic properties are the very important characteristics, and different characteristics of the particles can be obtained by different fabrication methods [52].

Iron oxide NPs are prepared and stored in colloidal form, so the stability of the particles is very important. The stability of the particles is determined by three forces: hydrophobic-hydrophobic forces, magnetic forces, and Van der Waals forces. The nanoparticles tend to aggregate due to the hydrophobic interactions, and micron clusters are formed from the aggregation [53]. The micron clusters continue to aggregate due to the magnetic dipole-dipole interactions, and they are magnetized by neighboring clusters. In an external magnetic field, the clusters are further

magnetized, and their aggregation increases. Because of the Van der Waals forces to minimize the total surface energy, the nanoparticles also aggregate in suspension. The clusters have low surface areas, have large volumes, and show ferromagnetic behavior. Therefore, the aggregation by these forces limits the applications of iron oxide NPs. Coatings (or stabilizer) are required to stabilize the iron oxide NPs [54]. Stabilizers, including surfactants and polymers, are usually added during the preparation process to prevent aggregation of the particles [55]. For biomedical applications, the ideal coating materials also should be biocompatible and biodegradable. The polymers generally adhere to the surfaces in a substrate-specific manner. Coatings also can protect the particles from further oxidization [56].

## 2.10. Green Synthesis

Green synthesis is the plant-mediated synthesis of nanoparticles that reduces the use of hazardous substances in the design, manufacture, and application of chemical products. The use of leaves, flower, stem, root or whole plant for the synthesis of NPs is considered to be a green approach [57-63]. Different researchers have reported the synthesis of IONPs using the green synthesis route. Demirezen et al. [57] have used *Ficus carica* (dried fruit extract) and ferric chloride hexahydrate to synthesize IONPs. The size of the nanoparticles was found to be  $9 \pm 4$  nm by TEM. Taib et.al [58] have used *Azadirachta indica* aqueous leaf extract as a reducing agent and stabilizing agent for the synthesis of stable IONPs. The presence of biomolecules like flavonoids and terpenoids of the aqueous leaf extract is found to play a major role in the formation of  $\text{Fe}_3\text{O}_4$ -NPs through infrared spectra analysis. TEM study inferred the size in the range of 9-14 nm. Kanagasubbulakshmi et.al [59] have utilized *Lagenaria siceraria* leaf extract for the green synthesis of IONPs and their characterization was done by UV-vis, SEM, EDX, XRD and FTIR. IONPs were found to be cubical in shape and size ranges from 30 nm-100 nm. The phytochemicals present in the leaf play a role as a reducing agent that assists in the synthesis of  $\text{Fe}_3\text{O}_4$ -NPs with increased antioxidant properties. An aqueous

extract of *Eriobotrya japonica* leaves was used by Onal et al [60], as a heterogeneous Fenton like catalyst for the green synthesis of IONPs. The NPs were characterized by XRD, FTIR and SEM and the results were found to be irregular spherical shaped nanoparticles and mainly consist of  $\gamma$ -Fe<sub>2</sub>O<sub>3</sub> and Fe<sub>3</sub>O<sub>4</sub> and iron oxyhydroxide (FeOOH) structures. The as-prepared IONPs were used as a heterogeneous catalyst for decolorisation of a toxic azo-dyestuff and basic red 46. *Platanus orientalis* leaf extract is elucidated by Sylvia Devi et al [61] for the green synthesis of IONPs. This leaf extract plays a dual role in reducing and capping agents for the preparation of IONPs. The authors have explained the role of the leaf extract in the fabrication of IONPs in this research. XRD inferred the existence of mixed-phase iron oxide of  $\alpha$ -Fe<sub>2</sub>O<sub>3</sub> and  $\gamma$ -Fe<sub>2</sub>O<sub>3</sub>. TEM estimated an average diameter of 38 nm for the as-prepared nanomaterial. As prepared IONPs show valuable

antifungal activity against *Aspergillus niger* and *Mucor piriformis*. Ag/Fe<sub>3</sub>O<sub>4</sub> nanocomposite was prepared by *Euphorbia peplus* Linn (L.) leaf extract as a suitable reducing source and stabilizing agent by Sajjadi et al [62]. TEM analysis inferred the spherical shape of Ag/Fe<sub>3</sub>O<sub>4</sub> nanocomposite with an average size of 5-10 nm. The as-prepared Ag/Fe<sub>3</sub>O<sub>4</sub> nanocomposite was employed as a magnetically recoverable catalyst for the [2+3] cycloaddition of arylcyanamides and sodium azide. This study reports a facile and eco-friendly approach for the ultrasound-assisted synthesis of silver and iron oxide nanoparticles and their enhanced antibacterial and antioxidant activities. The fenugreek seed extract was used as reducing, capping, and stabilizing agents for the synthesis of superparamagnetic IONPs by Deshmukh et al [63]. TEM study measured the particle size in the range of 20-40 nm. The fenugreek seed extract was confirmed as a reducing and capping agent

**Table 1.** Size/morphology and application of Fe<sub>3</sub>O<sub>4</sub>/Fe<sub>2</sub>O<sub>3</sub> nanomaterial prepared through green synthesis method

Material	Green Material used	Particle size/morphology	Applications	Ref.
Fe <sub>3</sub> O <sub>4</sub>	<i>Ficus carica</i> (common fig) dried fruit extract	9 ± 4 nm, spherical shapes with a monodisperse distribution	Biomedical	[57]
Fe <sub>3</sub> O <sub>4</sub>	<i>Azadirachta indica</i> leaf extract	9-14 nm, the shape was mostly spherical and oval	biomedical applications such as in targeting drug delivery system	[58]
Fe <sub>3</sub> O <sub>4</sub>	<i>Lagenaria siceraria</i> leaves extract	30 nm - 100 nm	MRI contrast enhancement, tissue repair, hyperthermia, drug delivery and in cell separation	[59]
$\gamma$ -Fe <sub>2</sub> O <sub>3</sub> and Fe <sub>3</sub> O <sub>4</sub>	<i>Eriobotrya japonica</i> leaves	30-100 nm by SEM analysis, irregular spherical shape	Heterogeneous catalyst	[60]
$\alpha$ -Fe <sub>2</sub> O <sub>3</sub> and $\gamma$ -Fe <sub>2</sub> O <sub>3</sub>	<i>Platanus orientalis</i> leaf extract	The spherical oxide particles have an average diameter of 38 nm	Antifungal activity against <i>Aspergillus niger</i> and <i>Mucor piriformis</i> .	[61]
Ag/Fe <sub>3</sub> O <sub>4</sub>	<i>Euphorbia peplus</i> Linn (L.) leaf extract	Spherical shaped nanocomposite with an average size of 5-10 nm	Magnetically recoverable catalyst for the [2+3] cycloaddition of arylcyanamides and sodium azide	[62]
Magnetic iron oxide	Fenugreek seed extract	Particle size in the range of 20-40 nm	antibacterial activities	[63]

by FTIR spectra. As prepared IONPs were used in antibacterial activities. The advantages of green synthesis over chemical and physical approaches are eco-friendliness, low cost, low energy, simple technique, non-toxic, and easy availability of the starting materials. The outcome of different researchers on the green synthesis of IONPs is summarized in Table 1.

### 3. CHARACTERIZATION

The size and shape of iron oxide nanoparticles (IONPs) are also very important parameters because they are not only related to the magnetic properties but also related to the applications of the particles. Size can also represent the crystalline part of the iron core, the whole iron core including both the crystalline and amorphous part, the core and the whole particle including both the core and the coating [64]. The particles also have a range of their size, so the size can represent the number, volume, or intensity-weighted mean size. TEM can be used to characterize the size and shape of the particles. The size of the particles can be determined by using High-resolution TEM. It also provides the details of the size distribution and the shape of the particles [65]. It can be used to study defects and surface atomic arrangement of the particles also, as it shows the arrangement of the atoms. XRD can be used to determine the crystalline structure of the particles [66]. In an XRD diffraction pattern, the intensity of the iron oxide peak can be used to determine the proportion of iron oxide formed in a mixture by comparing the experimental peak and reference peak intensities. The crystallite size of the crystal can be determined from the XRD analysis. Small-angle Neutron Scattering can be used to characterize the size, size distribution, shape, and structure of the particles. The surface morphology of the nanomaterials can be characterized by SEM study and EDX can be used for the compositional analysis. The specific surface area is measured by BET measurements and the FTIR is used to measure the functional groups.

The characterizations carried out by some of the researchers for IONPs are demonstrated herewith. Bhoj and Mandal [11] characterized the structure and crystallite size of  $\text{Fe}_2\text{O}_3$  nanopowders

with help of XRD. Figure 1 presents the X-ray diffractogram of  $\text{Fe}_2\text{O}_3$  nanopowders prepared by heating the polymeric precursor in the air at  $200^\circ\text{C}$  for 4h. XRD indicates the well-defined hexagonal shape with the R3C space group for the as-prepared materials. The average crystallite size,  $D$  was calculated with  $D2q1/2$  in the (110), (121), (120) and (220) etc prominent peaks of the diffractogram.

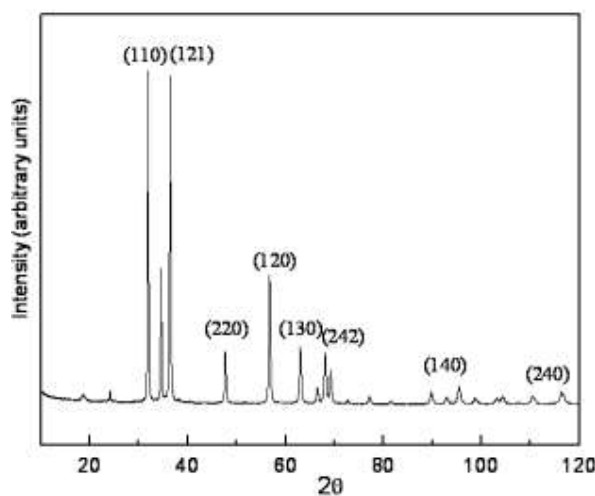


**Fig. 1.** The X-ray diffractograms of  $\text{Fe}_2\text{O}_3$  nanopowders processed by heating the polymeric precursor in air at  $200^\circ\text{C}$  for 4h. [Reproduced from Inter. J. Innovations & Advancement in Comp. Sci., 2015, 4, 12, Mandal et al.] [11].

$\text{Fe}_3\text{O}_4$ -C nanocomposite was characterized by Fichtner et al. [67] with the help of SEM and TEM. The SEM image of  $[\text{Fe}_3\text{O}_4\text{-C}]$  (Figure 2) demonstrates that the material consists of interlinked nanotubes and nanogranular structures. The tubes were determined with the diameter of the range between 10 and 100 nm with the lengths varied up to several micrometers. There were a large number of tubes encapsulated with  $\text{Fe}_3\text{O}_4$  nanoparticles at their tips, including some longer tubes within it. The presence of a core-shell structure is inferred with the TEM from the nanogranular region of the composite, containing  $\text{Fe}_3\text{O}_4$  cores with graphitic onions shells. The interface between graphitic carbon and  $\text{Fe}_3\text{O}_4$  with short-range disordered layers is observed. The  $\text{Fe}_3\text{O}_4$  particles were surrounded by around 8 layers of graphite with an average C-coating thickness of approximately 3 nm.





**Fig. 2.** SEM (top left) and TEM images of  $[\text{Fe}_3\text{O}_4\text{-C}]$ . [Reproduced from Beilstein J. Nanotechnol., 2013, 4, 699-704, Prakash R., Fanselau K., Ren S., Mandal T. K., Kübel C., Hahn H., Fichtner M] [67].

The IONPs were characterized by Sylvia Devi et al [61] applying XRD, SEM, TEM, EDX, IR and Uv-vis spectroscopy. XRD inferred the existence of mixed-phase iron oxide of  $\alpha\text{-Fe}_2\text{O}_3$  and  $\gamma\text{-Fe}_2\text{O}_3$ . The spherical oxide particles have an average diameter of 38 nm as measured from TEM. The green synthesized  $\text{Ag/Fe}_3\text{O}_4$  nanocomposite was characterized using XRD, field emission scanning electron microscope, TEM, EDX and FTIR spectroscopy by Sajjadi et al [62]. TEM analysis of  $\text{Ag/Fe}_3\text{O}_4$  nanocomposite showed the spherical shape NPs with an average size of 5-10 nm. Nanoparticles prepared by Demirezen [57] were characterized by XRD, EDX, TEM, UV-visible spectroscopy and FTIR. TEM images confirmed the size of the NPs prepared by them as  $9 \pm 4$  nm with a metallic core-oxide shell form. The nanoparticles were found in spherical shapes with a monodisperse distribution. Kayani et al. [33] characterized the sol-gel prepared  $\text{Fe}_2\text{O}_3$  NPs through XRD, FTIR, SEM, TGA/DTA-DSC and vibrating sample magnetometer. XRD study inferred the hematite phase of the as-prepared iron oxide NPs with an average crystallite size of the range from 34 to 36.7 nm [33].

#### 4. APPLICATIONS

Magnetic iron oxide nanomaterials (MIONs) with proper surface chemistry possess the interesting properties that can be utilized in a variety of

applications like biomedical (targeted drug delivery, MRI contrast agent, antibacterial, hyperthermia, and other cancer treatments), nanorobotics (treatment of diabetes, treatment of cancer, cellular nanosurgery and gene-therapy) and energy devices (Li-ion battery, supercapacitor and chemical sensor). Figure 3 summarizes the applications of magnetic iron oxide nanomaterials.



**Fig. 3.** The applications of magnetic iron oxide nanomaterials.

##### 4.1 Bio Medical

Magnetic iron oxide NPs (MIONs) have been intensively studied in several years for its applications in targeted drug delivery, MRI contrast agent, magnetic gels, magnetic recording media, ferrofluids, hypothermia cancer treatment and other biomedical applications [68]. Below a critical size, magnetic particles become a single domain in contrast with the usual multidomain structure of the bulk magnetic materials and exhibit unique phenomena such as superparamagnetism [69] and quantum tunneling of the magnetization [70-71].

MIONs have very important applications in the hyperthermia treatment process. Hyperthermia is an elevated body temperature condition owing to the failure of thermoregulation. If the elevated body temperatures are relatively high, hyperthermia is a medical emergency and requires immediate treatment. Hyperthermia can be created artificially by drugs or medical devices and hyperthermia therapy which are exploited to

treat some kinds of cancer and other conditions in conjunction with radiotherapy, chemotherapy or both. MIONs are mostly nanometer-sized ferrite nanoparticles of magnetite ( $\text{Fe}_3\text{O}_4$ ) or maghemite ( $\gamma\text{-Fe}_2\text{O}_3$ ) [72].

On exposure to an alternating magnetic field (AMF), MIONs create heat with the mechanisms of hysteresis loss and relaxational losses [72]. Hysteresis loss occurs in large MIONs which have multiple magnetic domains. Such MION particles on application to an AMF results in the orientation of the magnetic moments to align continuously with the direction of the magnetic field [Figure-4] [72]. This creates a difference in energy which is produced in the form of heat [73]. On decreasing MION sizes, the number of magnetic domains will also reduce until a single magnetic domain remains at a threshold size [74]. When the size is reached below this, MIONs are deemed superparamagnetic and in the presence of an AMF, heat is mainly generated by Néel relaxation and Brownian relaxation [76]. Néel relaxation refers to rapid changes in the particle's magnetic moment when treated

to AMF [Figure-4] [76]. The rapid realignment is opposed by the crystalline structure of the particles, resulting in heat production. Brownian relaxation refers to the frictional heat produced from the physical rotation of particles within a supporting medium when the particles attempt to realign themselves with the change in the magnetic field [Figure-4] [75-76]. More discussion on the mechanism of heating is reported by Ruta et al. elsewhere [77].

The MIONs with the size range of 10-20 nm found to show the best superparamagnetic properties. But with this size, the NPs face the problem of agglomeration. Coating of MIONs with biocompatible materials like peptides, lipids, and silica provides a good alternative to protect magnetic NPs. Different researchers studied on the coating of MIONs to obtain the best hyperthermia properties. Marziah et al. [78] applied the dendrimer nanopolymers for coating IONPs for the application in magnetic hyperthermia. They used the fourth-generation polyamidoamine dendrimer-coated IONPs ( $\text{G}_4\text{@IONPs}$ , particle size  $10 \pm 4$  nm) through the



**Fig. 4.** Heat generation mechanisms of magnetic NPs in response to an AMF. Green circles indicate MIONs, short straight arrows indicate magnetic field direction, curved arrows indicate the movement (solid curved arrow) or change in magnetic moment direction (dashed curved arrow) and dashed lines indicate domain boundaries in multidomain particles. Adapted from Suriyanto et al. Biomed. Eng. Online, 201, 16, 36 [76].

co-precipitation method. The cytotoxicity of  $G_4@IONPs$  with different concentrations was investigated in a human breast cancer cell line (MCF<sub>7</sub>) and human fibroblast cell line (HDF<sub>1</sub>). The in vitro toxicity assessments confirmed the low of the as-prepared NPs. Their results encouraged the future application of  $G_4@IONPs$  in magnetic hyperthermia [78]. Kandasamy et al [79] investigated the potential of magnetic hyperthermia using aminosilane-coated SPIONs in a glioblastoma tumor model. The magnetic hyperthermia was found to be effective for the therapeutic process of glioblastoma tumors in the animal models, using aminosilane-coated SPIONs with a high specific absorption rate [79]. Cheraghipour et al. [80] studied the citrate capped SPIONs, used for magnetic fluid hyperthermia therapy. Curcio et al [81] reported the design of an optimized nanohybrid for cancer tri-therapy,

featuring maghemite ( $\gamma\text{-Fe}_2\text{O}_3$ ) nanoflower-like multicore nanoparticles considered for efficient magnetic hyperthermia and a spiky copper sulfide shell (IONF@CuS) with a high near-infrared absorption coefficient suitable for photothermal and photodynamic therapy.

The effect of interparticle interactions on the hyperthermia properties of  $\text{Fe}_3\text{O}_4$  NPs was studied by Aslibeiki et al [82]. They found the increase in temperature with an increase in NPs in an AC magnetic field, e.g. the temperature increase of 7 nm particles obtained was 8 times more than that of 5 nm particles [82]. Ebrahimisadr et al observed the effect of concentration on magnetic hyperthermia properties of  $\text{Fe}_3\text{O}_4$  NPs (18 nm) prepared via co-precipitation method. The temperature rise of suspension in the AC magnetic field was found to increase sharply with increasing the NPs concentration [83]. Kandasamy et al [84]

**Table 2.** The summary of work of different researchers on hyperthermia

Material	Property improvements/ Applications	Ref
$\text{Fe}_3\text{O}_4$ NPs	Interparticle interactions influence the heat generation of NPs. They observed more temperature rise with more particle size.	[82]
$\text{Fe}_3\text{O}_4$ NPs	Effect of concentration on magnetic hyperthermia properties of $\text{Fe}_3\text{O}_4$ NPs. Mean diameter of NPs was at around 18 nm (SEM), The XRD study inferred the spinel structure of $\text{Fe}_3\text{O}_4$ , $\Delta T$ increased sharply with increase in the NPs concentration.	[83]
Fourth-generation dendrimer-coated iron-oxide nanoparticles ( $G_4@IONPs$ )	The cytotoxicity of $G_4@IONPs$ with different concentrations was assessed in a human breast cancer cell line (MCF <sub>7</sub> ) and human fibroblast cell line (HDF <sub>1</sub> ). The viability of MCF <sub>7</sub> cells incubated with $G_4@IONPs$ decreased significantly after magnetic hyperthermia.	[78]
Colloidal dispersion (Fe-raSpin <sup>TM</sup> R) of iron oxide cores	The influence of clustering on hyperthermia performance of iron oxide nanoparticles was studied. Iron oxide cores mean size 9 nm, varying cluster size was about 18-56 nm.	[85]
Iron oxide nanoparticles	Effect of assemblies of magnetic iron oxide nanoparticles in hyperthermia.	[86]
Iron oxide magnetic nanoclusters	The as obtained results confirmed the efficiency of the nanoclusters to generate the required intratumoral temperature after repeated injections and demonstrated that nanocluster-mediated magnetic hyperthermia significantly inhibits cancer growth.	[87]
Iron oxide nanoparticles	Heat transfer properties of iron oxide nanoparticles were investigated to study magnetic fluid hyperthermia, Magnetite nanoparticles with a median diameter of 13.8 nm fixed in an agar matrix showed a specific absorption rate of 5.6 W/g in a field of 5.0 kA/m, and a concentration of 5 wt.% was sufficient to increase the temperature above the temperature required for magnetic hyperthermia treatment.	[88]

studied the synthesis of hydrophilic and surface-functionalized SPIONs through coprecipitation/thermolysis methods followed by in situ surface functionalization with short-chained molecules for the treatment of liver cancer [84].

The influence of clustering on the hyperthermia performance of IONPs has been investigated by Bender et al [85] with a commercial colloidal dispersion (FeraSpin™R) of iron oxide cores (mean size about 9 nm) with varying cluster size

of 18-56 nm. They observed that clustering of the superparamagnetic cores leads to remanent magnetic moments within the large clusters. Because of the internal moment relaxation, the colloids with the large clusters excel in magnetic hyperthermia experiments [85].

Usov [86] studied that dilute assemblies of iron oxide NPs of optimal diameters are capable of providing SAR of the order of 400–600 W/g in AMF with the amplitude  $H_0 = 100$  Oe in the

**Table 3.** Clinical trials (randomized) on hyperthermia combined with radiotherapy, chemotherapy or chemotherapy/chemotherapy.

Type of Cancer	Number of patients (randomized)	Treatment type	Outcomes	Ref.
Squamous cell carcinoma of the thoracic esophagus undergoing	66	Control arm- Neoadjuvant chemo-radiotherapy & surgery Experimental arm- Neoadjuvant hyperthermochemoradiotherapy (capacitive system involving an intraluminal applicator, 42.5-44°C at tumor surface for 30 min & 6 sessions)	Complete response- 25% in experimental arm- 5.9% in control arm 3 year survival 50.4% experimental arm 24.2% control arm	[89]
Glioblastoma	79	Control arm- Radiotherapy & oral hydroxyurea & brachytherapy boost Experimental arm- Radiotherapy & oral hydroxyurea & brachytherapy boost & radiative hyperthermia, 915 MHz, $\geq 42.5^\circ\text{C}$ for 30 min, 15-30 min before and after brachytherapy)	Median survival- 76 weeks for control arm 85 weeks for hyperthermia arm $p = 0.02$	[90]
Localised high-risk soft-tissue sarcoma, extremity and retroperitoneal	341	Control arm- Neoadjuvant & adjuvant chemotherapy (etoposide, ifosfamide, doxorubicine) & local therapy (surgery +/- radiotherapy) Experimental arm: Neoadjuvant and adjuvant chemotherapy (etoposide, ifosfamide, doxorubicine) & local therapy (surgery +/- radiotherapy) & radiative hyperthermia, $42^\circ\text{C}$ for 60 min on first day and 4 of 3 weekly chemotherapy cycles for to 8 sessions)	Median follow-up 34 months significant improvement in local progression-free survival (hazard ratio = 0.58, $p = 0.003$ ) and disease-free survival (hazard ratio = 0.7, $p = 0.011$ )	[91]
Non-muscle-invasive bladder cancer (NMIBC)	190	The primary end point was 24-mo recurrence-free survival in the intention-to-treat and per-protocol analyses in all papillary NMIBC patients ( $n = 147$ ). Analyses done with the log-rank test and Fisher exact test. All tests were two-sided.	CHT is a safe and effective treatment option in patients with intermediate- and high-risk papillary NMIBC. A significantly higher 24-mo RFS in the CHT group was seen in the PP analysis.	[92]
NMIBC when bacillus Calmette-Guérin (BCG) fails.	104	Primary outcome measures were DFS and complete response at 3 mo for the CIS at randomization subgroup. The analysis was based on intention-to-treat.	There was no significant difference in DFS between treatment arms (hazard ratio 1.33, 95% confidence interval [CI] 0.84-2.10, $p = 0.23$ ).	[93]



frequency range  $f = 300\text{--}500$  kHz [86]. Albarqi et al [87] used cobalt- and manganese-doped, IONPs (CoMn-IONP) encapsulated in biocompatible PEG-PCL (poly(ethylene glycol)- b-poly( $\epsilon$ -caprolactone))-based nanocarriers to generate the required intratumoral temperature above  $40^\circ\text{C}$ . In the study of Yamamoto et al [88], IONPs were dispersed in an agar phantom in order to use them to mimic tumor tissue that is surrounded by normal tissue, to study magnetic fluid hyperthermia. Magnetite nanoparticles with a median diameter of 13.8 nm fixed in an agar matrix showed a specific absorption rate of 5.6 W/g in a field of 5.0 kA/m, and a concentration of 5 wt% was sufficient to increase the required temperature [88]. The observations of different researchers on hyperthermia are summarized in Table 2. A number of randomized clinical trials have been reported on the impact of hyperthermia on various cancers in combination with radiotherapy, chemotherapy or both with many studies recently in progress (Table 3).

Magnetic nanoparticles of  $\text{Fe}_3\text{O}_4$  are able to target cancerous cells and have potential use in cancer therapeutics [94–97]. Kyeong et al [98] reported the fabrication of  $\text{Fe}_3\text{O}_4$  NPs double-layered silica NPs with a silica core and highly packed  $\text{Fe}_3\text{O}_4$  NPs layers for Efficient Bio-Separation. A novel ideal multimodal contrast agent, MCAs ( $\text{F-AuNC@Fe}_3\text{O}_4$ ) were engineered by assembling Au nanocages and ultra-small iron oxide nanoparticles ( $\text{Fe}_3\text{O}_4$ ) for simultaneous  $T_1$ - $T_2$  dual MRI and CT contrast imaging [99]. The antimicrobial property of green synthesized  $\text{Fe}_3\text{O}_4$ -NPs [59] was investigated against Gram-negative - *Escherchia coli* and Gram positive- *Staphylococcus aureus*, The Zone of inhibition for this study was found to be 10 mm for *Escherchia coli* and 8 mm for *Staphylococcus aureus*. As prepared IONPs prepared through the green synthesis method by Sylvia Devi et al [61] show valuable antifungal activity against *Aspergillus niger* and *Mucor piriformis*. Nanorods of  $\text{g-Fe}_2\text{O}_3$  [100] and  $\text{a-Fe}_2\text{O}_3$  [101] fabricated through the hydrothermal method are used in biomedical and antibacterial activity respectively, while  $\text{g-Fe}_2\text{O}_3$  nanorods [102] prepared via co-precipitation method is used in bio-tagging.

#### 4.2. Nanorobotics

Nanorobotics is the technology of creating

robots at the nanoscale [103]. The names nanobots, nanoids, nanites or nanomites have also been used to describe these hypothetical devices currently under research and development. These nanoscale machines are very tiny stuff as small as the molecular size. So, it can enter the biological organ effectively and easily without any obstacles like the antibody response, because the size of the nano-machine is smaller than the antibody's size. If there is any antibody response, the nanorobot can get out of the antigen-antibody reaction. Nanorobot is applied in advanced medical applications like the detection and treatment of diabetes. It is also used in early detection and treatment of cancer, in cellular nanosurgery and genetherapy [103–104]. Because magnetism has been widely used in medical nanorobotics, MIONs, in particular, have shown to be well suited for this purpose. Sylvain Martel has reviewed the use of magnetic nanoparticles in the field of medical nanorobotics with some of the related main functionalities that can be embedded in nanorobotic agents [103].  $\text{Fe}_3\text{O}_4$  and  $\text{g-Fe}_2\text{O}_3$  in particular, are used extensively in medical nanorobotic applications due to their low toxicity and their known pathways of metabolism, making these materials attractive for nanorobotic agents designed for medical applications [103]. In medical nanorobotics,  $\text{Fe}_3\text{O}_4$  MIONs are generally preferred to  $\text{g-Fe}_2\text{O}_3$  MNP due to its higher saturation magnetization. The magnetization state for a ferromagnetic material is the result of the alignment of microscopic regions in the material known as magnetic domains or magnetic moments. Guiding magnetic iron oxide nanoparticles with the help of an external magnetic field to its target is the principle behind the development of superparamagnetic iron oxide nanoparticles (SPIONs) as novel drug delivery vehicles [104]. SPIONs are small synthetic  $\gamma\text{-Fe}_2\text{O}_3$  or  $\text{Fe}_3\text{O}_4$  particles with a core ranging between 10 nm and 100 nm in diameter. These magnetic particles are coated with certain biocompatible polymers, such as dextran or polyethylene glycol, which provide chemical handles for the conjugation of therapeutic agents and also improve their blood distribution profile. The recent research on SPIONs is increasing because of their use as diagnostic agents in magnetic resonance imaging



Fig. 5. A schematic diagram about medical nanorobot and its applications.

as well as for drug delivery vehicles. Delivery of anticancer drugs by coupling with functionalized SPIONs to their targeted site is one of the important areas of research in the development of cancer treatment methods [104]. A schematic diagram of medical nanorobot is presented in Figure 5. Magnetic helical nanorobots can perform 3D navigation in various liquids with a sub-micrometer precision under low-strength rotating magnetic fields ( $<10$  mT) [105]. Since magnetic fields with low strengths are harmless to cells and tissues, magnetic helical nanorobots are promising tools for biomedical applications, such as minimally invasive surgery, cell manipulation and analysis, and targeted therapy. Qiu and Nelson [105] checked on magnetic helical micro/nanorobots, including their fabrication, motion control, and further functionalization for biomedical applications. Nanoparticles with magnetic property can be used as the primary method of physically directing aptamer-MNPs and drug payloads to their target cells [106]. Aptamer-MNPs could act as nanosurgeons [106].

#### 4.3. Energy Devices

Nanocrystalline  $\alpha\text{-Fe}_2\text{O}_3$  based dye-sensitized solar cells (DSSC) with two different morphologies, such as nanorods and nanoparticles,

have been prepared by Manikandan et al applying one-pot low-temperature method [107]. The magnetic measurement revealed the ferromagnetic behavior of the as-prepared  $\alpha\text{-Fe}_2\text{O}_3$  samples. The DSSC based on the optimized  $\alpha\text{-Fe}_2\text{O}_3$  nanorods array reaches a conversion efficiency of 0.43%, which is higher than that obtained from  $\alpha\text{-Fe}_2\text{O}_3$  nanoparticles (0.29%) under the light radiation of  $1000 \text{ W/m}^2$  [107]. Core-shell  $\gamma\text{-Fe}_2\text{O}_3@\text{SnO}_2$  hollow nanoparticles have been synthesized by a low-cost and environmentally friendly seed-mediated hydrothermal method by Zhang et al [108]. The gas sensing tests of the  $\gamma\text{-Fe}_2\text{O}_3@\text{SnO}_2$  hollow NPs revealed that the samples exhibited fast response and recovery rates, which enable them to be promising materials for gas sensors. A facile and template-free greener route is used to fabricate natural polysaccharide-based biocompatible mesh-like  $\text{Fe}_2\text{O}_3/\text{C}$  nanocomposites for supercapacitor applications [109]. The nanocomposite prepared at  $500^\circ\text{C}$  with mesh-like structure reveals maximum specific capacitance of  $315 \text{ Fg}^{-1}$  in  $2 \text{ M KOH}$  solution at a scan rate of  $2 \text{ mVs}^{-1}$  and good capacity retention (88.9%) after 1500 continues charge-discharge cycles with energy density of  $37 \text{ Whkg}^{-1}$ , indicating that the  $\text{Fe}_2\text{O}_3/\text{C}$  composite can be used as a promising electroactive material for a supercapacitor. Umar and coworkers reported the synthesis

and characterizations of  $\alpha\text{-Fe}_2\text{O}_3$  hexagonal nanoparticles and their effective utilization for the smart chemical sensor applications [110]. The as-synthesized  $\alpha\text{-Fe}_2\text{O}_3$  nanoparticles were utilized as efficient electron mediators for the fabrication of 4-nitrophenol chemical sensor in aqueous media.

A new carbon encapsulated  $\text{Fe}_3\text{O}_4$  nanocomposite was synthesized by simple one-step pyrolysis of  $\text{Fe}(\text{CO})_5$  by Fichtner et al [67] for the Li-ion battery energy storage device application. The as-prepared  $\text{Fe}_3\text{O}_4/\text{C}$  nanocomposite electrode exhibited a stable reversible capacity of  $920 \text{ mAh} \cdot \text{g}^{-1}$  at  $93 \text{ mA} \cdot \text{g}^{-1}$  in the subsequent 50 cycles. The as-synthesized material could be used directly as an anode in a Li-ion cell and demonstrated a stable capacity, and good cyclic and rate performances. Nanocasting strategy is employed to tune the structure and size of  $\alpha\text{-Fe}_2\text{O}_3$  active nanoparticles as a promising anode material for Li-ion cells by Lupo et al [111].

Different group of researchers have also prepared  $\alpha\text{-Fe}_2\text{O}_3$  nanoparticles for the use of electrode material in Li-ion battery with different active material structure like, nano-flakes [112], mesoporous nano [113], spindle-like mesoporous [114], hollow spheres mesoporous shell [115], porous nanoflowers [116] and they reported different reversible capacity of their prepared material ( $680 \text{ mAh} \cdot \text{g}^{-1}$  @ 80 cycle [112],  $1293 \text{ mAh} \cdot \text{g}^{-1}$  @ 50 cycle [113],  $911 \text{ mAh} \cdot \text{g}^{-1}$  @ 50 cycle [114],  $830 \text{ mAh} \cdot \text{g}^{-1}$  @ 15 cycle [115],  $974 \text{ mAh} \cdot \text{g}^{-1}$  @ 1 cycle [116]). Superparamagnetic  $\text{Fe}_3\text{O}_4$  nanocrystals/graphene composites (FGC) were prepared and used as supercapacitors by Li et al [117]. The super capacitance values of the FGC composites were increased compared with those of the graphene sheets or  $\text{Fe}_3\text{O}_4$  NCs. A comprehensive design of carbon-encapsulated  $\text{Fe}_3\text{O}_4$  nanocrystals and their lithium storage properties have been reported by Song et al [118]. A high-performance supercapacitor-battery hybrid energy storage device based on graphene-enhanced electrode materials with ultrahigh energy density has been designed and fabricated by Zhang et al. [119]. The as-fabricated hybrid supercapacitor  $\text{Fe}_3\text{O}_4/\text{G}/3\text{DGraphene}$  demonstrated an ultrahigh energy density of  $147 \text{ Whkg}^{-1}$  (power density of  $150 \text{ Wkg}^{-1}$ ), which also remained of  $86 \text{ Whkg}^{-1}$

even at a high power density of  $2587 \text{ Wkg}^{-1}$ . A high-performance supercapacitor-battery hybrid energy storage device based on graphene-enhanced electrode materials with ultrahigh energy density  $\text{Fe}_3\text{N}$  surface-modified  $\text{Fe}_3\text{O}_4$  NPs with excellent lithium storage ability were reported by Li et al [120]. Uniform  $\text{Fe}_3\text{O}_4$  nanospheres with carbon matrix support for improved lithium storage capabilities were synthesized by Chen et al [121], with a reversible capacity of  $712 \text{ mAh} \cdot \text{g}^{-1}$  retained after 60 charge/discharge cycles, using one-pot synthesis method.  $\text{Fe}_3\text{O}_4@\text{C}$  microcapsules were prepared via two-step hydrothermal reactions by Yuan et al [122]. In  $\text{Fe}_3\text{O}_4@\text{C}$  microcapsules, mesoporous  $\text{Fe}_3\text{O}_4$  nanorods are coated with amorphous carbon layers. In Li test cells, the  $\text{Fe}_3\text{O}_4/\text{C}$  composites with such special structures demonstrate a high specific capacity and good cyclic stability as anode materials.

A high-density magnetic storage device material for the development of spintronics and RAM devices was reported by Tsuchiya et al. [123]. Deniz et al fabricated a heterojunction device of  $\text{Au}/\text{Fe}_3\text{O}_4$  NPs/n-Si/Al with the as-prepared  $\text{Fe}_3\text{O}_4$  nanoparticles (monodisperse 8 nm) [124].  $\text{Fe}_3\text{O}_4/\text{CNT}$  nanostructures were developed and exploited as anode catalysts in mediatorless microbial fuel cells (MFC) by Park et al [125].  $\text{Fe}_3\text{O}_4/\text{CNT}$  composite ( $\text{Fe}_3\text{O}_4$  NPs: 3~8-nm-sized) showed the maximum MFC power density of  $865 \text{ mW} \cdot \text{m}^{-2}$  associated with excellent durability performances.  $\text{FeO}/\text{Fe}_3\text{O}_4$  core-shell nanocubes have been investigated by Torruella et al [126].  $\text{Fe}_2\text{O}_3$  nanofilm semiconductor prepared by Pawar et al [127] is applied by them in the gas sensors.  $\text{Fe}_2\text{O}_3/\text{reduced graphene oxide (rGO)}$  nanocomposite [128] fabricated through hydrothermal method and mesoporous  $\text{g-Fe}_2\text{O}_3$  nanoparticle/Ketjen Black composite [129] prepared through a combination of solvothermal and precursor thermal route are applied in Li-ion battery.  $\text{Fe}_2\text{O}_3/\text{S}$  nanocomposite synthesized via the wet chemistry route by Zhao et al. [130] is used as the cathode in lithium-sulfur batteries.

Thus, the present review will shed more light on synthesis methods, nano-scale properties and applications of iron oxide nanomaterials. Different iron oxide nanostructures, properties, and applications are summarized in Table 5.

**Table 4.** A summary of the application of different iron oxide nanomaterials in energy devices

Nanostructure	Particle size/property	Application	Ref.
$\alpha$ -Fe <sub>2</sub> O <sub>3</sub> Nanorod & NPs	Ferromagnetic	DSSC	Manikandan et al [107]
Core-shell $\gamma$ -Fe <sub>2</sub> O <sub>3</sub> @SnO <sub>2</sub>	Samples exhibited fast response and recovery rates	Gas sensor	Zhang et al [108]
Fe <sub>2</sub> O <sub>3</sub> /C nanocomposites for	Electroactive material, specific capacitance of 315 Fg <sup>-1</sup> in 2 M KOH solution	Supercapacitor	Sethuraman et al [109]
Fe <sub>3</sub> O <sub>4</sub> /C nanocomposite	Electrode with reversible capacity of 920 mAh·g <sup>-1</sup> at 93 mA·g <sup>-1</sup> in the subsequent 50 cycles	Anode in Li-ion battery	Fichtner et al [67]
$\alpha$ -Fe <sub>2</sub> O <sub>3</sub>	Electroactive material	Anode in Li-ion battery	Lupo et al [111]
$\alpha$ -Fe <sub>2</sub> O <sub>3</sub> nano-flakes	Reversible capacity: 680 mA h g <sup>-1</sup> @ 80 cycle	Electrode in Li-ion battery	Reddy et al [112]
Mesoporous nano $\alpha$ -Fe <sub>2</sub> O <sub>3</sub>	Reversible capacity: 1293 mA h g <sup>-1</sup> @ 50 cycle	Electrode in Li-ion battery	Sun et al [113]
Spindle like mesoporous $\alpha$ -Fe <sub>2</sub> O <sub>3</sub>	Reversible capacity: 911 mA h g <sup>-1</sup> @ 50 cycle	Electrode in Li-ion battery	Xu et al [114]
Hollow spheres mesoporous shell $\alpha$ -Fe <sub>2</sub> O <sub>3</sub>	Reversible capacity: 830 mA h g <sup>-1</sup> @ 15 cycle	Electrode in Li-ion battery	Wu et al [115]
$\alpha$ -Fe <sub>2</sub> O <sub>3</sub> porous nanoflowers	Reversible capacity: 974 mA h g <sup>-1</sup> @ 1 cycle	Electrode in Li-ion battery	Zeng et al [116]
Fe <sub>3</sub> O <sub>4</sub> nanocrystals@graphene composites	Superparamagnetic	Supercapacitor	Li et al [117]
Fe <sub>3</sub> O <sub>4</sub> /G//3DGraphene hybrid	Graphene-enhanced electrode materials: Energy density: 147 W h kg <sup>-1</sup> , power density: 150 W kg <sup>-1</sup>	Supercapacitor	Zhang et al [119]
Fe <sub>3</sub> N surface-modified Fe <sub>3</sub> O <sub>4</sub> NPs	Electrode materials with ultrahigh energy density	Supercapacitor-battery hybrid energy storage device	Li et al [120]
Fe <sub>3</sub> O <sub>4</sub> nanospheres/Carbon	Enhanced lithium storage properties, reversible capacity of 712 mA h g <sup>-1</sup> retained after 60 cycles	Li storage material	Chen et al [121]
Fe <sub>3</sub> O <sub>4</sub> @C microcapsule	High specific capacity and good cyclic stability	Anode material	Yuan [122]
Fe <sub>3</sub> O <sub>4</sub> /CNT nanostructures	Fe <sub>3</sub> O <sub>4</sub> NPs (3~8-nm-sized), Power density of composite: 865 mW m <sup>-2</sup>	Anode catalysts in mediatorless microbial fuel cells	Park et al [125].



**Table 5.** A summary of different iron oxide nanostructures

Nanostructure	Fabrication Method	Particle size/ property	Application	Ref.
Flowerlike $\alpha$ -Fe <sub>2</sub> O <sub>3</sub> nanostructures	Solvothermal	High surface area	Adsorbent for the removal of As <sup>V</sup> and Cr <sup>VI</sup> from water	Cao et al [131]
g-Fe <sub>2</sub> O <sub>3</sub> nanorods	Hydrothermal	60 nm, super paramagnetic particles	Biomedical	Aghazadeh et al [100]
$\alpha$ -Fe <sub>2</sub> O <sub>3</sub> nanorods	Hydrothermal	Av. diameter: 10 to 35 nm	Antibacterial activity	Dawy et al [101]
Fe <sub>2</sub> O <sub>3</sub> nano-flakes	Solution combustion	17 nm, good optical absorbance and magnetic properties	Photocatalyst	Dhiman et al [132]
$\gamma$ -Fe <sub>2</sub> O <sub>3</sub> nanorods	Co-precipitation	18 nm, non-spherical	Bio-tagging	Layek et al [102]
a-Fe <sub>2</sub> O <sub>3</sub> nanoparticles	Solvent thermal	Size: about 5 nm, high specific surface area of ~162 m <sup>2</sup> /g	to remove arsenic in water	Tanga et al [133]
Fe <sub>2</sub> O <sub>3</sub> nanofilm	Screen printing	n-type semiconductor	Gas sensor	Nair et al [106]
Fe <sub>3</sub> O <sub>4</sub> & $\gamma$ -Fe <sub>2</sub> O <sub>3</sub>	Solvothermal	50-100 nm	Catalyst (used for degradation of diphenhydramine)	Pastrana-Martinez et al [134]
Fe <sub>2</sub> O <sub>3</sub> /reduced graphene oxide (rGO) nanocomposite	Hydrothermal	Av size: 9 nm, specific capacity maintained at 600 mAh/g after 70 cycles	Anode in Li-ion Battery	Sethuraman et al [109]
Mesoporous $\square$ -Fe <sub>2</sub> O <sub>3</sub> nanoparticle/Ketjen Black composite (KB)	Solvothermal + precursor thermal	Composite has nanoporous network and well-dispersed g-Fe <sub>2</sub> O <sub>3</sub> particles with a size of ca. 5 nm are embedded in the mesopores of KB	Anode in Li-ion Battery	Umar et al [110]
a-Fe <sub>2</sub> O <sub>3</sub> / polypyrrole (Py) nanocomposite	Chemical method	Size decreases from 20 to 5 nm by increasing Py content from 5 to 25%	Photocatalyst (applied for degradation of methylene blue)	Harraz et al [135]

Nanostructure	Fabrication Method	Particle size/ property	Application	Ref.
Fe <sub>2</sub> O <sub>3</sub> /S nanocomposite	Wet chemistry	Porous Fe <sub>2</sub> O <sub>3</sub> acts as an internal polysulfide reservoir. A stable reversible discharge capacity of 574.3mAh/g was obtained after 50 cycles	Cathode for lithium-sulfur batteries	Xu et al [114]
$\alpha$ -Fe <sub>2</sub> O <sub>3</sub> Nanorod & NPs	Low-temperature method	Ferromagnetic	DSSC	Manikandan et al [107]
Core-shell $\gamma$ -Fe <sub>2</sub> O <sub>3</sub> @SnO <sub>2</sub>	Hydrothermal	Samples exhibited fast response and recovery rates	Gas sensor	Zhang et al [108]
Fe <sub>2</sub> O <sub>3</sub> /C nanocomposites for	Green route	Electroactive material, the specific capacitance of 315 Fg <sup>-1</sup> in 2 M KOH solution	Supercapacitor	Sethuraman et al [109]
Fe <sub>3</sub> O <sub>4</sub> /C nanocomposite	Pyrolysis	Electrode with reversible capacity of 920 mAh·g <sup>-1</sup> at 93 mA·g <sup>-1</sup> in the subsequent 50 cycles	Anode in Li-ion battery	Fichtner et al [67]
Fe <sub>3</sub> O <sub>4</sub> nanospheres/Carbon	One-pot synthesis	Enhanced lithium storage properties, a reversible capacity of 712 mAh g <sup>-1</sup> retained after 60 cycles	Li storage material	Chen et al [121]
Fe <sub>3</sub> O <sub>4</sub> @C microcapsule	Hydrothermal	High specific capacity and good cyclic stability	Anode material	Yuan [122]
Fe <sub>3</sub> O <sub>4</sub> and $\alpha$ -Fe <sub>2</sub> O <sub>3</sub> NPs	Hydrothermal	Fe <sub>3</sub> O <sub>4</sub> : 5 nm; $\alpha$ -Fe <sub>2</sub> O <sub>3</sub> : 20 nm First-discharge capacities: Fe <sub>3</sub> O <sub>4</sub> = 1,380 mAhg <sup>-1</sup> , $\alpha$ -Fe <sub>2</sub> O <sub>3</sub> 1,280 mAhg <sup>-1</sup>	Anode in Li-ion battery	Lou et al [22]
Fe <sub>3</sub> O <sub>4</sub> /C nanocomposite	Hydrothermal	Ferromagnetic	Removes pollutant Cr(VI) ions and Rhodamine B from wastewater	Chen et al [24]

## 5. CONCLUSIONS

Magnetic iron oxide nanomaterials (MIONs) can potentially be used as magnetic targeted drug delivery carriers and magnetic resonance imaging contrast agents due to their high saturation magnetization, low toxicity, and biocompatibility. It has been observed that the magnetic properties of  $\text{Fe}_3\text{O}_4$  nanoparticles can be tailored by their particle sizes, size distributions, microstructures and surface morphologies which are possible by exploring advanced synthesis methods. Iron oxide nanomaterials have been reported to be prepared through coprecipitation, hydrothermal, sol-gel, microemulsions, polyol, electrochemical, aerogel and sonolysis methods. But, chemical methods have been seen to produce iron oxide nanomaterials with desired properties and applications. During the last few years iron oxides are very widely used as photocatalyst for the photocatalytic degradation of organic dyes due to their high photosensitive nature. Thus, iron oxide nanomaterials can be utilized for the environmental purification of polluted water. It has also been used in nanomedicines, in MRI and in energy harvesting devices. Iron oxide nanomaterials prepared through modified novel chemical methods and green synthesis routes can be utilized on large scale in nanomedicines, in photocatalysis, and in energy devices. The present review summarizes that flowerlike  $\alpha\text{-Fe}_2\text{O}_3$  nanostructures with high surface area, prepared by Cao et al are attractive adsorbent for the removal of  $\text{As}^{\text{V}}$  and  $\text{Cr}^{\text{VI}}$  from water. The functionalized magnetic nanoparticles of  $\text{g-Fe}_2\text{O}_3$ , prepared by Ali and Venkataraman, have many applications in site-specific drug delivery, MRI, magnetic gels, cancer treatment and other biomedical applications. Mesoporous  $\text{g-Fe}_2\text{O}_3$  nanoparticle/Ketjen Black composite, reported by Dong et al, is used as anode material for Li-ion batteries with improvement in electronic conductivity and structure stability of  $\text{g-Fe}_2\text{O}_3$ . Ni-Co ferrite synthesized by Brito et al is utilized in sensor applications.  $\text{Fe}_3\text{O}_4$  prepared by Diniz et al, via the combustion method, are reported to be promising materials for application in biomedicine. Porous  $\text{Fe}_2\text{O}_3$  prepared by Zhao et al, through the wet chemistry method, is used as

a cathode for lithium-sulfur batteries. However, better synthesis routes can be tried to find out for the synthesis of iron oxide nanomaterials with advanced applications of it. Different preparation methods lead to different phases and different degrees of size control. Thus, the correlation of the preparation process with size and magnetic properties is still a challenge.

Despite recent progress on the synthesis and application of iron oxide nanomaterials, there are many gaps in the development of materials for the use in biomedical, nanorobots and energy devices. The application of target-oriented drug delivery and nanorobots is still a challenge. Till now, much of the research conducted in the area of nanorobotics remains highly theoretical, possibly because of the difficulties in fabricating such devices. But, nature's biological nanorobotic systems do exist and provide evidence that such systems are at least possible, so more efforts should be employed on the application of nanorobots in the biological context of nanomedicines. Therefore, biological systems could be better exploited and for that extensive research on biological structures and application of nanotechnology with these structures to be experimented. As limited research has been carried out on targeted and effective drug delivery vehicles, more and more investigations are required including the synthesis of new drug delivery vehicles for therapeutic, imaging and diagnostic purposes. Also very few reports are available for the synthesis of iron oxide nanomaterials using green synthesis route. Therefore, environment friendly green synthesis methods to be more focused for the preparation of magnetic iron oxide nanomaterials. Work on the application of iron oxide nanomaterials in solar energy devices, is not done effectively. So, the work on the development of iron oxide nanomaterials and its nanocomposites for the better use in solar energy devices can also be extended.

## REFERENCES

1. Weinstein, J. S., Varallyay, C. G., Dosa, E., Gahramanov, S., Hamilton, B., Rooney, W. D., Muldoon, L. L., and Neuwelt, E. A., "Superparamagnetic Iron Oxide Nanoparticles: Diagnostic Magnetic Resonance Imaging and Potential Therapeutic Applications in

- Neurooncology and Central Nervous System Inflammatory Pathologies”, A Review. *J. Cerebral Blood Flow & Metabolism*, 2010, 30, 15-35.
2. Laurent, S., and Mahmoudi, M., “Superparamagnetic Iron Oxide Nanoparticles: Promises for Diagnosis and Treatment of Cancer”. *Int. J. Mol. Epidemiol. Genet.*, 2011, 2, 367-390.
3. Namvar, F., Rahman, H. S., Mohamad, R., Baharara, J., Amini, M., Stanley, chartr, M., and Yeap, S. K., “Cytotoxic Effect of Magnetic Iron Oxide Nanoparticles Synthesized Via Seaweed Aqueous Extract”. *Int. J. Nanomedicine*, 2014, 9, 2479-2488.
4. Awwad A. M., Nidá, and Salem, M., “A Green and Facile Approach for Synthesis of Magnetic Nanoparticles”. *J. Nanosci. Nanotechnol.*, 2012, 2, 208-213.
5. Ansari, S. A. M. K, Ficiara, E., Ruffinatti, F. A., Stura, I., Argeniano, M., Abollino, O., Cavalli, R., Guiot, C. and Agata, F. D., “Magnetic Iron Oxide Nanoparticles: Synthesis, Characterization and Functionalization for Biomedical Applications in the Central Nervous System”. *J. Materials*, 2019, 12, 465, 1-24.
6. Teja, Amyn, S, and Koh, P. Y., “Synthesis Properties and Applications of Magnetic Iron Oxide Nanoparticles. *J. Progress in Crystal Growth and Characterization of Materials*”, 2009, 55, 22-45.
7. Chatterjee, J, Haik, Y., and Chen, C. J., “A Biocompatible Magnetic Film: Synthesis and Characterization”. *Journal of Magnetism and Magnetic Materials*, 2004, 257, 113-118.
8. Indira, T. K, and Lakshmi, P. K., “Magnetic Nanoparticles A Review”. *Intern. J. Pharma. Sci. Nanotechno*, 2010, 3, 1035-1042.
9. Alagiri, M, and Hamid, S. B. A., “Green synthesis of  $\alpha$ -Fe<sub>2</sub>O<sub>3</sub> Nanoparticles for Photocatalytic Application”. *J. Mater. Sci: Mater Electron*, 2014, 25, 3572-3577.
10. Shiomi, D, Sato, K., and Takui, T., “Spin-Spin Correlation Function and Magnetic Susceptibility of Quantum Ferrimagnetic Spin Chains as Models for Organic Molecule-Based Ferrimagnetics”. *J. Physical Chemistry*, 2000, 104, 9, 1961-1965.
11. Bhoj, G., and Mandal, T. K., “Synthesis and XRD Study of Fe<sub>2</sub>O<sub>3</sub> Nanoparticles Prepared by A Chemical Route”. *Inter. J. Innovations & Advancement in Comp. Sci.*, 2015, 4, 2347-8616.
12. Mahdavi, M., Namvar, F., Ahmad, M. B., and Mohamad, R., “Green Biosynthesis and Characterization of Magnetic Iron oXide (Fe<sub>3</sub>O<sub>4</sub>) Nanoparticles Using Seaweed (Sargassum muticum) Aqueous Extract”. *J. Molecules.*, 2013, 18, 5954-5964.
13. Tendo, F., Ngenefeme, J., Namanga., Eko, J., Mbom, Y. D., Tantoh, N. D., and Rui, K. W. M., “A One Pot Green Synthesis and Characterization of Iron Oxide Pectin Hybrid Nanocomposite”. *Open J. Composite Mater.* 2013, 3, 30-37.
14. Laurent, S., Forge, D., Port, M., Roch, A., Robic, C., Elst, L. V., and Muller, R. N., “Magnetic Iron Oxide Nanoparticles: Synthesis, Stabilization, Vectorization, Physicochemical Characterizations and Biological Applications”. *Chemical Reviews*, 2008, 108, 2064-2110.
15. Benyettou, F., Milosevic, I., Olsen, J. C., Motte, L., and Trabolsi, A., “Ultra Small Superparamagnetic Iron Oxide Nanoparticles Made to Order”. *J. Bionalysis & Biomedicine*, 2012, S5, 006, 1-6.
16. Wang, Z., Zhao, L., Yang, P., Lv, Z., Sun, H., and Jiang, Q., “Water-Soluble Amorphous Iron Oxide Nanoparticles Synthesized by A Quickly Pestling and Nontoxic Method at Room Temperature as MRI Contrast Agent”. *J. Chem. Engg.*, 2014, 235, 231-235.
17. Wu, W., He, Q. G., and Jiang, C. Z., “Magnetic Iron Oxide Nanoparticles: Synthesis and Surface Functionalization Strategies”. *J. Nanoscale Res. Lett.*, 2008, 3, 397-415.
18. Zhu, H., Yang, D., and Zhu, L., “Transparent, Thermally and Mechanically Stable Super Hydrophobic Coating Prepared by an Electrochemical Template Strategy”. *J. Material Chemistry A.*, 2015, 3, 3801-3807.
19. Ge, S., Shi, X., Sun, K., Li, C., Uher, C., Jr, J. R. Baker., Holl, M. M. B., and Orr, B. G., “Facile Hydrothermal Synthesis of Iron Oxide Nanoparticles with Tunable Magnetic Properties”. *J. Physical Chemistry C.*, 2009, 113, 13593-13599.
20. Haw, C. Y., Mohamed, F., Chia, C. H., Radiman, S., Zakaria, S., Huang, N. M., and Lim, H., “Hydrothermal Synthesis of Magnetite Nanoparticles as MRI Contrast Agents”. *Ceram. Intern.*, 2010, 36, 1417-1422.
21. Li, J., Zheng, L., Cai, H., Sun, W., Shen, M., Zhang, G., and Shi, X., “Facile One Pot Synthesis of Fe<sub>3</sub>O<sub>4</sub> Composite Nanoparticles Fordual Mode MR/CT Imaging Applications”. *J. ACS Appl. Mater. Interfaces*, 2013, 5, 10357-10366.
22. Lou, X., Huang, J., Li, T., Hu, H., Hu, B., and Zhang, Y., “Hydrothermal Synthesis of Fe<sub>3</sub>O<sub>4</sub> and A-Fe<sub>2</sub>O<sub>3</sub> Nanocrystals as Anode Electrode Materials for Rechargeable Li-Ion Batteries”. *J. Mater. Sci: Mater Electro.*, 2014, 25, 1193-1196.
23. Liu, X. D., Chen, H., Liu, S. S., Ye, L. Q., and Li, Y. P., “Hydrothermal Synthesis of Superparamagnetic Fe<sub>3</sub>O<sub>4</sub> Nanoparticles with



- Ionic Liquids as Stabilizer". *J. Bull.*, 2015, 62, 217-221.
24. Chen, M., Shao, L. L., Li, J. J., Pei, W. J., Chen, M. K., and Xie, X. H., "One-Step Hydrothermal Synthesis of Hydrophilic  $\text{Fe}_3\text{O}_4$ /Carbon Composites and Their Application in Removing Toxic Chemicals". *RSC Adv.*, 2016, 6, 35228-35238.
  25. Razik, A. A., Nassar, M. Y., Elazeem, Abd., Sharkwy, M. El., Amin, A. S., and Lateif, E. A. A., "Preparation and Characterization Of A-Fe O Via Auto-Combustion Synthesis". *Intern. J. of Mater. Res., E-First Article*, 2018, 5, 252-255.
  26. Hyeon, T., Lee, S. S., Park, J., Chung, Y., and Na, H. B., "Synthesis of Highly Crystalline and Monodisperse Maghemite Nanocrystallites without Size-Selection Process". *J. Amer. Chem. Soc.*, 2001, 123, 12798-12801.
  27. Jolivet, J. P., Vassiere, L., Chaeneac, C., and Tronc, E., "Magnetic Iron Oxide Nanoparticles: Synthesis, Characteristics, Magnetic Behavior, and Biomedical Applications". *J. E. Mater. Res. Soc. Sympo. Proceed.*, 1997, 432, 145.
  28. Massart, R., Roger, J. and Cabuil, V., "New Trends in Chemistry of Magnetic Colloids: Polar and Non Polar Magnetic Fluids, Emulsions, Capsules and Vesicles". *Brazilian J. Phys.*, 1995, 25, 135-141.
  29. Woo, K., Hong, J., and Ahn, J. P., "Synthesis and Surface Modification of Hydrophobic Magnetite to Processible Magnetite Silica Propylamine". *J. Magnetism and Magnetic Materials*, 2005, 293, 177-181.
  30. Park, J., Lee, E., Hwang, N. M., Kang, M., Kim, S. C., Hwang, Y., Park, J. G., Noh, H. J., Kim, J. W., Park, J. H., and Hyeon, T., "One Nanometer-Scale Size Controlled Synthesis of Monodisperse Magnetic Iron Oxide Nanoparticles". *Angewandte Chemie Intern. Ed.*, 2005, 44, 2873-2877.
  31. Li, Z., Sun, Q., and Gao, M., "Preparation of Water soluble magnetite nanocrystals from Hydrated Ferric salts in 2-Pyrrolidone: mechanism leading to  $\text{Fe}_3\text{O}_4$ ". *Angewandte Chemie Intern. Ed.*, 2005, 44, 123-126.
  32. Reda, S. M., "Synthesis of  $\text{ZnO}$  and  $\text{Fe}_2\text{O}_3$  Nanoparticles by Sol-Gel Method and Their Application in Dye-Sensitized Solar Cells". *Materials Science in Semiconductor Processing*, 2010, 13, 417-425.
  33. Kayani, Z. N., Arshad, S., Riaz, S., and Naseem, S., "Synthesis of Iron Oxide Nanoparticles by Sol-Gel Technique and Their Characterization. *IEEE Transactions on Magnetics*", 2014, 8, 1-4.
  34. Raja, K., Mary, J., Jose, M., Verma, S., Prince, A. M., Ilangovan, K., Sethusankar, K., and Jerome, D., "Sol-Gel Synthesis and Characterization of A- $\text{Fe}_2\text{O}_3$  Nanoparticles". *J. Superlattices and Microstructures*. 2015, 86, 306-312.
  35. Sunder, S., Venkatachalam, G., and Kwon, S. J., "Sol-Gel Mediated Greener Synthesis of G- $\text{Fe}_2\text{O}_3$  Nanostructures for the Selective and Sensitive Determination of Uric Acid and Dopamine". *J. Catalysts*, 2018, 8, 1-17.
  36. Tartaj, P., Morales, M. P., Veintemillas-Verdaguer, S., Gonzales-Carreno, T. T., and Serna, J. C., "The Preparation of Magnetic Nanoparticles for Applications in Biomedicine". *J. Physics D: Applied Physics*, 2003, 36, 182-197.
  37. Pileni, M. P., "Reverse Micelles as Microreactors". *J. Physical Chem.*, 1993, 97, 6961-6973.
  38. Gupta, A. K., and Wells, S., "Surface Modified Superparamagnetic Nanoparticles for Drug Delivery: Preparation, Characterization, and Cytotoxicity Studies". *IEEE Transactions on Nanobioscience*, 2004, 3, 66-73.
  39. Jiang, W., Lai, K. L., Hu, H., Zeng, X. B., Lan, F., Liu, Ke. X., Yao, W., and Gu, Z. W., "The Effect of Iron Oxide Molar Ratio and Iron Salts Concentration on the Properties of Superparamagnetic Iron Oxide Nanoparticles in the Water System". *J. Nanoparticle Research*, 2011, 13, 5135-5145.
  40. Munshi, N., De, T. K., and Maitra, A., "Size Modulation of Polymeric Nanoparticles Under Controlled Dynamics of Microemulsion Droplets. *Journal of Colloid and Interface Science*", 1997, 190, 387-391.
  41. Park, J., Lee, E., Hwang, N. M., Kang, M., Kim, S. C., Huang, J. G., Park, G., Noh, H. J., Kim, J. H., Park, J., and Hyeron, H., "One Nanometer Scale Size Controlled Synthesis of Monodisperse Magnetic Iron Oxide Nanoparticles". *Angewandte Chemie Intern. Ed.*, 2005, 44, 123.
  42. Gavilan, H., Brollo, M. E. F., Gutierrez, L., Veintemillas-Verdaguer, S., and Morales, M. del, P., "Controlling the Size and Shape of Uniform Magnetic Iron Oxide Nanoparticles for Bio Medical Applications", *Clinical Applications of Magnetic Nanoparticles*, ed. N. T. K. Thanh, London, UK, 2018, 138, 68-104.
  43. Wan, J., Cai, W., Feng, J., Meng, X., and Liu, E., "In-situ Decoration of Carbon Nanotubes with Nearly Monodisperse Magnetite Nanoparticles in Liquid Polyols". *J. Mater. Chem.*, 2007, 17, 1188-1192.
  44. Jun, Y. W., Huh, Y. M., Choi, J. S., Lee, J. H., Song, H. T., Kim, S., Yoon, S., K. Kim, S., Shin, J. S., Suh, J. S., and Cheon, J., "Nanoscale Size Effect of Magnetic Nanocrystals and Their Utilization

- for Cancer Diagnosis Via Magnetic Resonance Imaging". *J. Amer. Chem. Soc.*, 2005, 127, 5732-5733.
45. Cabrera, L., Gutierrez, S., Menendez, N., Morales, M. P., and Herrasti, P., "Magnetite Nanoparticles: Electrochemical Synthesis and Characterization". *Journal of Magnetite Nanoparticles*, 2008, 53, 3436-3441.
46. Park, H., Ayala, P., Deshusses, Marc, A., Mulchandani, A., Choi, H., and Myung, Nosang, V., "Electrodeposition of Maghemite ( $\gamma$ - $\text{Fe}_2\text{O}_3$ ) Nanoparticles". *J. Chem. Engineering*, 2008, 139-1, 208-212.
47. Tavakoli, A., Sohrabi, M., and Kargari, A., "A Review of Methods for Synthesis of Nanostructured Metals with Emphasis on Iron Compounds". *J. Chemical Papers*, 2007, 61, 151-170.
48. Sabino, V. V., Maria, Del, Puerto, M., Oscar, B. M., Carmen, B., Xinqing, Z., Pierre, B., Pérez, de, A. Rigoberto, Jesus, R. C., Martin, S., Francisco, J. T. C., and Joaquin, F., "Colloidal Dispersions of Maghemite Nanoparticles Produced by Laser Pyrolysis with Application as NMR Contrast Agents". *J. Phys. D: Appl. Phys.*, 2004, 37, 2054-2059.
49. Mukh-Qasem, R. A., and Gedanken, A., "Sonochemical Synthesis of Stable Hydrosol of  $\text{Fe}_3\text{O}_4$  Nanoparticles". *Journal of Colloid and Interface Science*, 2005, 284, 489-494.
50. Kim, E. H., Lee, H. S., Kwak, B. K., and Kim, B. K., "Synthesis of Ferrofluid with Magnetic Nanoparticles by Sonochemical Method for MRI Contrast Agent". *Journal of Magnetism and Magnetic Materials*, 2005, 289, 328-330.
51. Corr, S. A., Gunko, Y. K., Douvalis, A. P., Venkatesan, M., Gunning, R. D., and Nellist, P. D., "From Nanocrystals to Nanorods: New Iron Oxide-Silica Nanocomposites from Metallorganic Precursors". *J. Phys. Chem. C*, 2008, 112, 1008.
52. Wang, C. T., and Ro, S. H., "Nanocluster Iron Oxide-Silica Aerogel Catalysts for Methanol Partial Oxidation". *J. Appl. Catal. A: General*, 2005, 285, 196-204.
53. Bagwe, R. P., Kanicky, J. R., Palla, B. J., Patanjali, P. K., and Shah, D. O., "Improve Drug Delivery Using Microemulsions: Rationale, Recent Progress, and New Horizons". *J. Critical Reviews in Therapeutic Drug Carrier Systems*, 2001, 18, 77-140.
54. Pileni, M. P., "Reverse Miscelles as Microreactors". *J. Physical. Chem.*, 1993, 97, 6961-6973.
55. Lawrence, M. J., and Rees, G. D., "Microemulsions Based Media as Novel Drug Delivery Systems". *J. Advanc. Drug Delivery Rev.*, 2012, 64, 175-193.
56. Fendler, J. H., "Atomic and molecular Clusters in Membrane Mimetic Chemistry". *J. Chemical Review*, 1987, 87, 877-899.
57. Demirezen, D. A., Yildiz, Y. S., Yilmaz, S., and Yilmaz, D. D., "Green Synthesis and Characterization of Iron Oxide Nanoparticles Using Ficus Carica (Common Fig) Dried Fruit Extract", *Journal of Bioscience and Bioengineering*. 2019, 127, 2, 241-245.
58. Taib, N. I., Latif, F. A., Mohamed, Z., and Zambri, N. D. S., "Green Synthesis of Iron Oxide Nanoparticles ( $\text{Fe}_3\text{O}_4$ -NPs) Using Azadirachta Indica Aqueous Leaf Extract", *International Journal of Engineering & Technology*, 2018, 7, 9-13.
59. Kanagasubbulakshmi, S., and Kadirvelu, K., "Green Synthesis of Iron Oxide Nanoparticles Using Lagenaria Siceraria and Evaluation of its Antimicrobial Activity", *Defence Life Science Journal*, 2017, 2, 4, 422-427.
60. Onal, E. S., Yatkin, T., Ergut, M., and Ozer, A., "Green Synthesis of Iron Nanoparticles by Aqueous Extract of Eriobotrya Japonica Leaves as a Heterogeneous Fenton-like Catalyst: Degradation of Basic Red 46". *International J. Chemical Engineering and Applications*, 2017, 8, 5, 327-333.
61. Sylvia Devi, H., Ahmad Boda, M., Ashraf Shah, M., Parveen, Sh. and Wani, A. H., "Green synthesis of Iron Oxide Nanoparticles Using Platanus Orientalis Leaf Extract for Antifungal Activity". *Green Process Synth*, 2019, 8, 38-45.
62. Sajjadi, M., Nasrollahzadeh, M., and Sajadi, S. M., "Green Synthesis of  $\text{Ag}/\text{Fe}_3\text{O}_4$  Nanocomposite Using Euphorbia Peplus Linn Leaf Extract and Evaluation of its Catalytic Activity". *Journal of Colloid and Interface Science*, 2017, 497, 1-13.
63. Deshmukh, A. R., Gupta, A. and Kim, B. S., "Ultrasound Assisted Green Synthesis of Silver and Iron Oxide Nanoparticles Using Fenugreek Seed Extract and Their Enhanced Antibacterial and Antioxidant Activities". *BioMed Research International*, 2019, 1-14.
64. Sugimoto, T., "Preparation of Monodispersed Colloidal Particles". *J. Adv. Colloid Interface Sci.*, 1987, 28, 65-108.
65. Kim, D. K., Zhang, Y., Voit, W., Rao, K. V., and Muhammed, M., "Synthesis and Characterization of Surfactant-Coated Superparamagnetic Monodispersed Iron Oxide Nanoparticles". *J. Magnetism and Magnetic Materials*, 2001, 225, 30-36.

66. Tang, J., Myers, M., Bosnick, K. A., and Brus, L. E., "Magnetite  $\text{Fe}_3\text{O}_4$  Nanocrystals: Spectroscopic Observation of Aqueous Oxidation Kinetics". *J. Physical Chem. B*, 2003, 107, 7501-7506.
67. Prakash, R., Fanselau, K., Ren, S., Mandal, T. K., Kübel, C., Hahn, H., and Fichtner, M., "A Facile Synthesis of A Carbon-Encapsulated  $\text{Fe}_3\text{O}_4$  Nanocomposite and its Performance as Anode in Lithium-Ion Batteries". *Beilstein J. Nanotechnol.*, 2013, 4, 699-704.
68. Fu, Chengyin, and Ravindra, Nuggehalli, M., "Magnetic Iron Oxide Nanoparticles: Synthesis and Applications". *J. Bioinspired, Biomimetic and Nanobiomaterials*, 2012, 1, 229-244.
69. Kittel, C., "Theory of the Structure of Ferromagnetic Domains in Films and Small Particles". *Physical Rev.*, 1946, 70, 965-971.
70. Chudnovsky, E. M, and Gunther, L., "Quantum Theory of Nucleation in Ferromagnets". *Physical Rev. B*, 1988, 37, 9455-9459.
71. Chudnovsky, E. M, and Gunther, L., "Quantum Tunneling of Magnetization in Small Ferromagnetic Particles". *Physical Rev. Lett.*, 1988, 60, 661-664.
72. Chang, D, Lim, M., Goos, A.C.M. J., Quiao, R., YeeNG, Y., Mansfeld, M.J., Davis, Thomas P., and Kavallaris, M., "Biologically Targeted Magnetic Hyperthermia: Potential and limitations". *Front Pharmacol.*, 2018, 9, 831.
73. Kirschning A, Kupracz L., and Hartwig J., "New Synthetic Opportunities in Miniaturized Flow Reactors with Inductive Heating". *Chem. Lett.*, 2012, 41, 562-570.
74. Houlding, Rebrov, Houlding T. K., and Rebrov E. V., "Application of Alternative Energy forms in Catalytic Reactor Engineering". *Green Process Synth.*, 2012, 1, 19-31.
75. Suto, M, Hirota, Y., Mamiya, H., Fujita, A., Kasuya, R., and Tohji, K., "Heat Dissipation Mechanism of Magnetite Nanoparticles in Magnetic Fluid Hyperthermia". *J. Magn. Magn. Mater.*, 2009, 321, 1493-1496.
76. Suriyanto, Ng E. Y, and Kumar, S. D., "Physical Mechanism and Modeling of Heat Generation and Transfer in Magnetic Fluid Hyperthermia Through Neelian and Brownian Relaxation: A Review". *Biomed. Eng. Online*, 2017, 16, 1-22.
77. Ruta, S., Chantrell, R., and Hovorka, O., "Unified Model of Hyperthermia Via Hysteresis Heating in Systems of Interacting Magnetic Nanoparticles". *Sci. Rep.*, 2015, 5, 9090.
78. Marzieh, Salimi, Sarkar, S., Saber, R., Delavari, Hamid, Alizadeh, Ali Mohammad, and Mulder, H. T., "Magnetic Hyperthermia of Breast Cancer Cells and MRI Relaxometry with Dendrimer-Coated Iron-Oxide Nanoparticles". *Cancer Nanotechnology*, 2018, 9, 1-19.
79. Kandasamy, G, Sudame, A., Luthra, T., Saini, K., and Maity, D., "Therapeutic Evaluation of Magnetic Hyperthermia Using  $\text{Fe}_3\text{O}_4$ -Aminosilane-Coated Iron Oxide Nanoparticles in Glioblastoma Animal Model". *Einstein São Paulo*, 2019, 17, 4, 1-9.
80. Cheraghipour, E, Javadpour, S., and Mehdizadeh, A. R., "Citrate Capped Superparamagnetic Iron Oxide Nanoparticles Used for Hyperthermia Therapy". *J. Biomedical Science and Engineering*, 2012, 5, 715-719.
81. Curcio, A, Silva, A. K. A., Cabana, S., Espinosa, A., Baptiste, B., Menguy, N., Wilhelm, C., and Abou-Hassan, A., "Iron Oxide Nano Flowers Cus Hybrids for Cancer Tri-Therapy: Interplay of Photothermal Therapy, Magnetic Hyperthermia and Photodynamic Therapy". *Theranostics*, 2019, 9, 1288-1302.
82. Aslibeiki, B., Ehsani, M. H., Nasirzadeh, F. and Mohammadi, M. A., "The Effect of Interparticle Interactions on Spin Glass and Hyperthermia Properties of  $\text{Fe}_3\text{O}_4$  Nanoparticles". *Materials Research Express*, 2017, 4, 7.
83. Ebrahimisadr, S., Aslibeiki, B., and Asadi, R., "Magnetic Hyperthermia Properties of Iron Oxide Nanoparticles: The Effect of Concentration". *Physica C: Superconductivity and its Applications*, 2018, 549, 119-121.
84. Kandasamy, G, Sudame, A., Luthra, T., Saini, K., and Maity, D., "Functionalized Hydrophilic Superparamagnetic Iron Oxide Nanoparticles for Magnetic Fluid Hyperthermia Application in Liver Cancer Treatment". *ACS Omega*, 2018, 3, 3991-4005.
85. Bender, P., Fock, J., Hansen, M. F., Bogart, L. K., Southern, P., Ludwig, F., Wiekhorst, F., Szczerba, W., Zeng, L. J., Heinke, D., Gehrke, N., Díaz, MTF., González-Alonso, D., Espeso, J. I., Fernández, J. R., and Johansson, C., "Influence of Clustering on the Magnetic Properties and Hyperthermia Performance of Iron Oxide Nanoparticles". *Nanotechnology*, 2018, 29, 1-13.
86. Usov, N. A., "Iron Oxide Nanoparticles for Magnetic Hyperthermia". *SPIN*, 2019, 09, 02.
87. Albarqi, H. A, Wong, L. H., Schumann, C., Sabei, F. Y., Korzun, T., Li, X., Hansen, M. N., Dhagat, P., Moses, A. S., Taratula, O., and Taratula, O., "Biocompatible Nanoclusters with High Heating Efficiency for Systemically Delivered Magnetic Hyperthermia". *ACS Nano*, 2019, 6, 6383-6395.
88. Yoshiyuki, Y., Tatsuhiro, I., and Takayuki, I., "A Heat Dissipation Study of Iron Oxide

- Nanoparticles Embedded an Agar Phantom for the Purpose of Magnetic Fluid Hyperthermia". *J. Nanoscience and Nanotechnology*, 2019, 19, 9, 469-5475.
89. Kitamura, K, Kuwano, H., Watanabe, M., Nozoe, T., Yasuda, M., and Sumiyoshi, K., "Prospective Randomized Study of Hyperthermia Combined with Chemoradiotherapy for Esophageal Carcinoma". *J. Surg. Oncol.*, 1995, 60, 55-58.
  90. Sneed, P. K, Stauffer, P. R., Mcdermott, M. W., Diederich, C. J., Lamborn, K. R., and Prados, M. D., "Survival Benefit of Hyperthermia in A Prospective Randomized Trial of Brachytherapy Boost +/- Hyperthermia for Glioblastoma Multiforme". *Int. J. Radiat. Oncol. Biol. Phys.*, 1998, 40, 287-295.
  91. Issels, R. D, Lindner, L. H., Verweij, J., Wust, P., Reichardt, P., and Schem, B. C., "Neo-adjuvant Chemotherapy Alone or With Regional Hyperthermia for Localised High-Risk Soft-Tissue Sarcoma: A Randomised Phase 3 Multicentre Study". *Lancet Oncol.*, 2010, 11, 561-570.
  92. Arends, T. J, Nativ, O., Maffezzini, M., de, Cobelli, O., Canepa, G., Verweij, F., Moskovitz, B., van der, Heijden, AG., and Witjes, JA., "Results of a Randomised Controlled Trial Comparing Intravesical Chemohyperthermia with Mitomycin C Versus Bacillus Calmette-Guérin for Adjuvant Treatment of Patients with Intermediate- and High-risk Non-Muscle-invasive Bladder Cancer". *Eur Urol.*, 2016, 6, 1046-1052.
  93. Tan, W. S., Panchal, A., Buckley, L., Devall, AJ., Loubière, L. S., Pope, A. M., Feneley, M. R., Cresswell, J., Issa, R., Mostafid, H., Madaan, S., Bhatt, R., McGrath, J., Sangar, V., Griffiths, TRL., Page, T., Hodgson, D., Datta, S. N., Billingham, L. J., and Kelly, J. D., "Radiofrequency-induced Thermo-chemotherapy Effect Versus a Second Course of Bacillus Calmette-Guérin or Institutional Standard in Patients with Recurrence of Non-muscle-invasive Bladder Cancer Following Induction or Maintenance Bacillus Calmette-Guérin Therapy (HYMN): A Phase III, Open-label, Randomised Controlled Trial". *Eur Urol.*, 2019, 75, 1, 63-71.
  94. Sindura, C. S, Babu, and N. C., Vinod, "Unbounding the Future: Nanobiotechnology in Detection and Treatment of Oral Cancer". *J. Adv. Med. Dent. Sci.*, 2013, 1, 66-77.
  95. Pal, D. K, and Nayak, A. K., "Nanotechnology for Targeted Delivery in Cancer therapeutics". *Intern. J. Pharmaceutical Sci. Rev. Res.*, 2010, 1, 1-7.
  96. Guardia, P., Corato, R. D., Lartigue, L., Wilhelm, C., Espinosa, A., Garcia-Hernandez, M., Gazeau, F., Manna, L., and Pellegrino, T., "Heat-Generating Iron Oxide Nanocubes: Subtle "Destructurators" of The Tumoral Microenvironment". *ACS Nano*, 2014, 6, 4268-4283.
  97. Zhao, H., Yuan, X., Yu, J., Huang, Y., Shao, Chen, Xiao, F., Lin, Li, Li, Y., and Tian, L., "Magnesium-Stabilized Multifunctional DNA Nanoparticles for Tumor-Targeted and Ph-Responsive Drug Delivery". *J. Advanc. Mater. Res.*, 2018, 10, 15418-15427.
  98. Kyeong, S, Jeong, C., Kang, H., Cho, H. J., Park, S. J., Yang, J. K., Kim, S., Kim, H. M., Jun, B. H., and Lee, Y. S., "Double-Layer Magnetic Nanoparticle-Embedded Silica Particles for Efficient Bio-Separation". *Plos One.*, 2015, 10, 1-12.
  99. Wang, G, Gao, W., Zhang, X., Mei, X., "Au Nanocage Functionalized with Ultra-Small Fe<sub>3</sub>O<sub>4</sub> Nanoparticles for Targeting T<sub>1</sub>-T<sub>2</sub> Dual MRI and CT Imaging of Tumor". *Sci Rep.*, 2016, 6, 1-10.
  100. Aghazadeh, M, and Aghazadeh, Fatemeh., "Magnetic Helical Micro-and Nanorobots: Toward Their Biomedical Applications". *J. Appl. Chem. Res.*, 2015, 1, 021-026.
  101. Dawy, M., El-Mahy, Safaa, K., Abd, and El, Aziz, E., "Synthesis, Characterization and Electrical Properties of A- Fe<sub>2</sub>O<sub>3</sub> Nanoparticle". *Australian J. Basic and Appl. Sci.*, 2012, 6, 55-62.
  102. Layek, S., Pandey, A., Pandey, A., and Verma, H. C., "Synthesis of Γ-Fe<sub>2</sub>O<sub>3</sub> Nanoparticles with Crystallographic and Magnetic Texture". *Intern. J. Advances in Engg & Techno.*, 2010, 2, 33-39.
  103. Martel, S., "Magnetic Nanoparticles in Medical Nanorobotics". *J. Nanoparticle Res.* 2015, 17, 1-15.
  104. Wahajuddin, S. A., and Arora, S., "Superparamagnetic Iron Oxide Nanoparticles: Magnetic Nanoplatforms as Drug Carriers". *I. J. Nanomedicine*, 2012, 7, 3445-3471.
  105. Qiu, F., and Nelson, B. J., "Magnetic Helical Micro and Nanorobots: Toward Their Biomedical Applications". *J. Engineering*, 2015, 1, 21-26.
  106. Nair, B. G, Nagaoka, Y., Morimoto, H., Yoshida, Y., Maekawa, T., and Kumar, D. S., "Aptamer Conjugated Magnetic Nanoparticles as Nanosurgeons". *Nanotechnology.*, 2010, 21, 448421-455102.
  107. Manikandan, A., Saravanan, A., Antony, S. A., and Bououdina, M., "One-Pot Low Temperature Synthesis and Characterization Studies of Nanocrystalline A-Fe<sub>2</sub>O<sub>3</sub> Based Dye Sensitized Solar Cells". *J. Nanosci. Nanotechno.*, 2015, 15, 4358-4366.
  108. Zhang, S., Ren, F., Wu, W., Zhou, J., Xiao, X.,



- Sun, L., Liu, Y., and Jiang, C., "Controllable Synthesis of Recyclable Core-Shell  $\Gamma$ - $\text{Fe}_2\text{O}_3$ @ $\text{SnO}_2$  Hollow Nanoparticles with Enhanced Photocatalytic and Gas Sensing Properties". *J. Physical Chem. Chemical Phys.*, 2013, 15, 8228-8236.
109. Sethuraman, B., Purushothaman, K. K., and Muralidharan, G., "Synthesis of Mesh-Like  $\text{Fe}_2\text{O}_3/\text{C}$  Nanocomposite Via Greener Route for High Performance Supercapacitors". *RSC Advances*, 2014, 4, 4631-4637.
  110. Umar, A. M., Akhtar, S., Dar, G. N., and Baskoutas, S., "Low-Temperature Synthesis Of  $\alpha$ - $\text{Fe}_2\text{O}_3$  Hexagonal Nanoparticles for Environmental Remediation and Smart Sensor Applications". *J. Talanta*, 2013, 116, 1060-1066.
  111. Lupo, F. D., Gerbaldi, C., Casino, S., Francia, C., Meligrana, G., Tuel, A., and Penazzi, N., " $\alpha$ - $\text{Fe}_2\text{O}_3$  Lithium Battery Anodes by Nanocasting Strategy from Ordered 2D And 3D Templates". *J. Alloys and Compounds*, 2014, 615, S482-S486.
  112. Reddy, M. V., Yu, T., Sow, C. H., Shen, Z. X., Lim, C. T., Subba, Rao, G. V., and Chowdhari, B. V. R., " $\alpha$ - $\text{Fe}_2\text{O}_3$  Nanoflakes as an Anode Material for Li-Ion Batteries". *Adv. Funct. Mater.*, 2007, 17, 2792-2799.
  113. Sun, B., Horvat, J., Kim, H. S., Kim, W. S., Ahn, J., Wang, G., "Synthesis of Mesoporous  $\alpha$ - $\text{Fe}_2\text{O}_3$  Nanostructures for Highly Sensitive Gas Sensors and High Capacity Anode Materials in Lithium Ion Batteries". *J. Phys. Chem. C*, 2010, 114, 18753-18761.
  114. Xu, X., Cao, R., and Jeong, S., "Spindle-like Mesoporous  $\alpha$ - $\text{Fe}_2\text{O}_3$  Anode Material Prepared from MOF Template for High-Rate Lithium Batteries". *J. Cho, Nano Lett.*, 2012, 12, 4988-4991.
  115. Wu, Z., Yu, K., Zhang, S., Xie, Y., "Hematite Hollow Spheres with A Mesoporous Shell: Controlled Synthesis and Applications in Gas Sensor and Lithium Ion Batteries". *J. Phys. Chem. C*, 2008, 112, 11307-11313.
  116. Zeng, S., Tang, K., Li, T., Liang, Z., Wang, D., Wang, Y., Qi, Y., and Zhou, W., "Facile Route for the Fabrication of Porous Hematite Nanoflowers: Its Synthesis, Growth Mechanism, Application in the Lithium Ion Battery, and Magnetic and Photocatalytic Properties". *J. Phys. Chem. C*, 2008, 112, 4836-4843.
  117. Li, B., Cao, H., Shao, J., Qu, M., and Warner, J. H., "Superparamagnetic  $\text{Fe}_3\text{O}_4$  Nanocrystals@ Grapheme Composites for Energy Storage Devices". *J. Mater. Chem.*, 2011, 21, 5069-5075.
  118. Song, K., Lee, Y., Jo, M. R., Nam, K. M., and Kang, Y. M., "Comprehensive Design of Carbon-Encapsulated  $\text{Fe}_3\text{O}_4$  Nanocrystals and Their Lithium Storage Properties". *J. Nanotechnology*, 2012, 23, 1-7.
  119. Zhang, F., Zhang, T., Yang, X., and Chen, Y., "A High-Performance Super Capacitor-Battery Hybrid Energy Storage Device Based on Graphene-Enhanced Electrode Materials with Ultrahigh Energy Density". *Energy Environmental Sci.*, 2013, 6, 1623-1632.
  120. Li, Y., Yan, Y., and Ming, H., "One-Step Synthesis  $\text{Fe}_3\text{N}$  Surface-Modified  $\text{Fe}_3\text{O}_4$  Nanoparticles with Excellent Lithium Storage Ability". *J. Zheng, Appl. Surf. Sci.*, 2014, 305, 683-688.
  121. Chen, J. S., Zhang, Y., and Lou, X. W., "One-Pot Synthesis of Uniform  $\text{Fe}_3\text{O}_4$  Nanospheres with Carbon Matrix Support for Improved Lithium Storage Capabilities". *ACS Appl. Mater. Interfaces*, 2011, 3, 3276-3279.
  122. Yuan, S. M., Li, J. X., Yang, L. T., Su, L. W., Liu, L., and Zhou, Z., "Preparation and Lithium Storage Performances of Mesoporous  $\text{Fe}_3\text{O}_4$ @C Microcapsules". *ACS Appl. Mater. Interfaces*, 2011, 3, 705-709.
  123. Tsuchiya, T., Terabe, K., Ochi, M., Higuchi, T., Osada, M., Yamashita, Y., Ueda, S., and Aono, M., "In Situ Tuning of Magnetization and Magnetoresistance in  $\text{Fe}_3\text{O}_4$  Thin Film Achieved with All-Solid-State Redox Device". *ACS Nano*, 2016, 10, 1655-1661.
  124. Deniz, A. R., Çaldıran, Z., Metin, O., Meral, K. K., and Aydoğan, S., "The Investigation of The Electrical Properties of  $\text{Fe}_3\text{O}_4/\text{N-Si}$  Heterojunctions in A Wide Temperature Range", *J. Colloid Interface Sci.*, 2016, 473, 172-181.
  125. Park, I. H., Kim, P., Kumar, G. G., and Nahm, K. S., "The Influence of Active Carbon Supports Toward the Electrocatalytic Behavior of  $\text{Fe}_3\text{O}_4$  Nanoparticles for the Extended Energy Generation of Mediatorless Microbial Fuel Cells". *Appl. Biochem. Biotechnol.*, 2016, 179, 1170-1183.
  126. Torruella, P., Arenal, R., Peña, F. D. L., Saggi, Z., Yedra, L., Eljarrat, A., Conesa, L. L., Estrader, M., Ortega, A. L., Alvarez, G. S., Nogués, J., Ducati, C., Midgley, P. A., Peiró, F., AND Estradé, S., "3D Visualization of the Iron Oxidation State in  $\text{FeO}/\text{Fe}_3\text{O}_4$  Core-Shell Nanocubes from Electron Energy Loss Tomography". *Nano Lett.*, 2016, 16, 5068-5073.
  127. Pawar, N. K., Kajale, D. D., Patil, G. E., Wagh, V. G., Gaikwad, V. B., Deore, M. K., and Jain, G. H., "Nanostructured  $\text{Fe}_2\text{O}_3$  Thick Film as an Ethanol Sensor". *Int. J. On Smart Sensing and Intelligent Systems*, 2012, 5, 441-457.

128. Zhou, W., Ding, C., Jia, X., Tian, Y., Guan, Q., and Wen, G., "Self-Assembly of  $\text{Fe}_2\text{O}_3$ /Reduced Graphene Oxide Hydrogel for High Li-Storage. Mater". Res. Bulletin, 2015, 7, 27502-27510.
129. Dong, H., Xu, Y., Ji, M., Zhang, H., Zhao, Z., and Zhao, C., "High Performance of Mesoporous  $\gamma\text{-Fe}_2\text{O}_3$  Nanoparticle/Ketjen Black Composite as Anode Material for Lithium Ion Batteries". J. Electrochimica Acta, 2015, 151, 118-125.
130. Zhao, C., Shen, C., Xin, F., Sun, Z., and Han, W., "Prussian Blue-Derived  $\text{Fe}_2\text{O}_3$ /Sulfur Composite Cathode for Lithium-Sulfur Batteries". Mater. Letters, 2014, 137, 52-54.
131. Cao, C. Y., Qu, J., Yan, W. S., Zhu, J. F., Wu, Z. Y., Song, W. G., "Low-Cost Synthesis of Flowerlike  $\alpha\text{-Fe}_2\text{O}_3$  Nanostructures for Heavy Metal Ion Removal: Adsorption Property and Mechanism". Langmuir, 2012, 28, 4573-4579.
132. Dhiman, P., Kumar, A. and Singh, M., "Solution Combustion Preparation of  $\text{Fe}_2\text{O}_3$ -Nano-Flakes: Synthesis and Characterization. Adv". Mat. Lett., 2012, 3, 330-333.
133. Tanga, W., Li, Q., Gao, S., and Shang, J. K., "Arsenic (III, V) Removal from Aqueous Solution by Ultrafine  $\alpha\text{-Fe}_2\text{O}_3$  Nanoparticles Synthesized from Solvent Thermal Method". J. Hazardous Mater., 2011, 192, 131-138.
134. Pastrana-Martinez Luisa, M., Pereira, Nuno, Lima, Rui, Faria, Joaquim L., Gomes, Helder, T., and Silva Adrian, M. T., "Degradation of Diphenhydramine by Photo-Fenton Using Magnetically Recoverable Iron Oxide Nanoparticles as Catalyst". Chemical Engineering Journal, 2015, 261, 45-52.
135. Harraz, F. A., Ismail, A. A., Al-Sayari, S. A., and Al-Hajry, A., "Novel- $\text{Fe}_2\text{O}_3$ /Polypyrrole Nanocomposite with Enhanced Photocatalytic Performance". J. Photochemistry and Photobiology A: Chemistry, 2015, 299, 18-24.